Tracing Dust Input to the Global Ocean using Thorium Isotopes in Marine Sediments: ThoroMap

S. S. Kienast[1], G. Winckler[2,3], J. Lippold[4,5] , S. Albani[6,7], and N.M. Mahowald[6]

[1] Department of Oceanography, Dalhousie University, Halifax, Nova Scotia, Canada

[2] Lamont-Doherty Earth Observatory, Columbia University, Palisades, NY, USA

[3] Department of Earth and Environmental Sciences, Columbia University, NY, USA

[4] Institute of Geological Sciences and Oeschger Centre for Climate Change Research, University of Bern, Switzerland

[5] Institute of Earth Sciences, University of Heidelberg, Germany

[6] Department of Earth and Atmospheric Sciences, Cornell University, Ithaca, NY, USA

[7] Institute for Geophysics and Meteorology, University of Cologne, Germany

Corresponding author: Stephanie Kienast (stephanie.kienast@dal.ca)

Key Points:

- Continental dust input to the ocean is reconstructed using Thorium isotopes
- A new global database of dust fluxes is presented for the late Holocene and the last Glacial Maximum
- Comparisons with recent coupled models identify regions of good model-data agreement

This article has been accepted for publication and undergone full peer review but has not been through the copyediting, typesetting, pagination and proofreading process which may lead to differences between this version and the Version of Record. Please cite this article as doi: 10.1002/2016GB005408

Abstract

Continental dust input into the ocean-atmosphere system has significant ramifications for biogeochemical cycles and global climate, yet direct observations of dust deposition in the ocean remain scarce. The long-lived isotope thorium-232 (^{232}Th) is greatly enriched in upper continental crust compared to oceanic crust and mid-ocean ridge basalt (MORB)-like volcanogenic material. In open ocean sediments, away from fluvial and ice-rafted sources of continental material, ^{232}Th is often assumed to be of predominantly eolian origin. In conjunction with flux normalization based on the particle reactive radioisotope thorium-230 (^{230}Th), ^{232}Th measurements in marine sediments are a promising proxy for dust accumulation in the modern and past ocean. Here we present ThoroMap, a new global data compilation of ^{230}Th-normalized fluxes of ^{232}Th. After careful screening, we derive dust deposition estimates in the global ocean averaged for the late Holocene (0-4 ka) and the Last Glacial Maximum (LGM, 19-23 ka). ThoroMap is compared with dust deposition estimates derived from CCSM3 and CCSM4, two coupled atmosphere, land, ocean, and sea-ice models. Model-data correlation factors are 0.63 (CCSM3) and 0.59 (CCSM4) in the late Holocene and 0.82 (CCSM3) and 0.83 (CCSM4) in the LGM. ThoroMap is the first compilation that is built on a single, specific proxy for dust and that exclusively uses flux-normalization to derive dust deposition rates.

1 Introduction

Continental dust, or mineral aerosol, plays a significant role in the climate system. Dust particles affect the Earth's radioactive balance by both scattering and absorbing incoming solar radiation and outgoing planetary radiation (e.g., Boucher et al., 2013). Additionally, dust-particles act as cloud condensation nuclei, and feldspars, in particular, as ice nuclei (Atkinson et al., 2013); clouds in turn affect planetary albedo. Dust deposition to snow and ice surfaces can significantly increase their melting rates by decreasing their albedo (Conway et al, 1996). Last but not least, iron-bearing dust profoundly influences the biological uptake of CO_2 not only in the terrestrial biosphere but also in large parts of the ocean where dissolved iron has unequivocally been shown to limit phytoplankton production (e.g., Boyd et al., 2007).

Many lines of evidence suggest that mineral dust has been an important player in the unperturbed climate system in the past, and that it will be one in the future (e.g., Werner et al. 2002, Mahowald et al., 2006, Martinez-Garcia et al., 2009, 2011; Winckler et al. 2005, 2008, 2016; Maher et al. 2010, Booth et al., 2012, Jaccard et al., 2013, Lamy et al. 2014, and others). Dust deposition in the mouth of the Senegal River increased sharply with the onset of commercial agriculture in the Sahel region ~ 200 years ago (Mulitza et al., 2010), and paleo data suggest large increases in desert dust over much the globe in the 20th century (Mahowald et al., 2010). Furthermore, satellite based studies suggest substantial dust emissions due to land use perturbation, making future increases in desert dust likely (Ginoux et al., 2012; Ward et al. 2014). Given that the overall radiative effect of dust in the atmosphere is likely negative and leading to cooling, increased dust concentrations in the atmosphere have the potential to mask future warming. However, studies on the effects of future climate change on dust loadings in the atmosphere give diverging results, resulting in an overall "low confidence" rating of climate change predictions of mineral dust in the recent IPCC reports (Boucher et al., 2013). Indeed, mineral dust and the uncertainties it introduces to our understanding of total aerosol radiative forcing and climate projections have been identified as critical research areas by the IPCC.

In addition to dust load (concentration) in the atmosphere, dust deposition is an important element of the dust cycle. However, direct measurements of dust deposition rates, in particular over the open ocean, are currently scarce. The lack of observations is exacerbated by the fact that numerical model estimates of dust deposition vary greatly, especially over remote oceanic areas (Schulz et al., 2012, Albani et al., 2014). Future evaluations and improvements of numerical models that quantify different features of the global dust cycle therefore require an adequate set of observations from the modern and past environment.

In marine sediments, ^{232}Th, a long-lived isotope of purely continental origin is often analyzed in conjunction with ^{230}Th, an isotope produced in sea-water at a constant and well-known rate by decay of uranium-234 (^{234}U). Thorium is one of the most particle reactive elements in sea-water, and is quickly scavenged onto sinking particles and exported to the sea floor (Bacon et al, 1984; Francois et al., 2004, 2007). Assuming that the flux of scavenged ^{230}Th to the sea floor is equal to its rate of production from ^{234}U-decay, there is a simple inverse relationship between the total flux of material accumulating on the seafloor and its concentration of scavenged ^{230}Th. This inverse relationship forms the basis of the ^{230}Th

normalization method, which is increasingly considered to yield more accurate reconstructions of bulk particles fluxes to the sea floor than the traditional age model-based mass accumulation rate (MAR) approach (e.g., François et al. 2004, 2007; McGee et al., 2010; Marcantonio et al., 2014). To derive the ^{230}Th-normalized flux of a sedimentary component, the bulk flux is multiplied with the concentration of the variable of interest, i.e., ^{232}Th in this study.

Together, ^{232}Th and ^{230}Th thus offer a promising proxy to reconstruct dust deposition in the ocean over millennial and glacial-interglacial time scales. Indeed, this approach is increasingly used in paleoceanographic studies (Adkins, 2006; Bradtmiller et al., 2007; Pourmand et al. 2004, Anderson et al., 2006, McGee et al., 2007, 2013; Winckler et al., 2008; Martínez-García et al., 2009; Woodard et al., 2012; Kienast et al., 2013, Serno et al., 2014; Lamy et al., 2014; Jacobel, et al. 2016, Costa et al., 2016).

Here, we compile Th data from the published literature from marine sediment cores and systematically explore the utility of ^{232}Th as a proxy for continental and dust inputs to the global ocean. The objective of this study is threefold. First, this work aims to increase spatial coverage of ^{232}Th deposition records, and to delineate the boundary between purely eolian and mixed continental inputs. Secondly, we combine the marine sediment data and results from climate modeling into a common framework, to identify areas in which model-based and sediment based estimates of dust deposition are comparable. The focus is on the late Holocene (0-4 ka) time slice, but data for the Last Glacial Maximum (LGM, 19-23 ka) are also presented. Ultimately, the goal of this study is to provide observations from the past environment that will help to improve the predictive capabilities of the dust cycle component in global scale coupled models.

The paper is organized as follows. First, we summarize the background on the use of ^{232}Th as continental proxy and the underlying assumptions (*section 2*). The methodological approach (*section 3*) describes the assembly of the full database and the filters applied to exclude sites influenced by non-eolian continental material. In section 4, Th-based dust fluxes are presented for the 0-4 ka and the 19-23 ka time-slice, and these estimates are compared with recent results from global coupled models (CCSM4 and CCSM3, Albani et al., 2014 and Mahowald et al. 2006, respectively).

2 Background

Thorium-232 is also known as primordial thorium because of its very long half-life (1.4×10^{10} yrs). Thorium-232 makes up almost all naturally occurring thorium in the Earth System, with other isotopes occurring only in trace amounts and as relatively short-lived decay products of the ^{238}U, ^{235}U and ^{232}Th decay series. After ^{232}Th, ^{230}Th is the next most stable isotope with a half-life of 75,584 ± 110 years (Cheng et al., 2013). We use ^{230}Th to normalize fluxes of ^{232}Th to the sea floor (*section 1*).

Th-232 is used as a dust proxy because its average concentration in upper continental crust (10.5-10.7 ppm, Taylor and McLennan, 1985; Rudnick and Gao, 2004, Fig. 1) is roughly 50 times greater than that in mid-ocean ridge basalt (MORB)-like material (0.14-0.28 ppm; Klein 2004, Kelemen et al., 2004). When the Earth' s mantle is melted and magma forms, trace elements display a preference for either the melt phase (magma) or the solid phase, i.e, the minerals that crystallize from the magma as it slowly cools. The relatively large size (10^{-10} m) and high charge (+4) of thorium ions render them incompatible with mafic and intermediate minerals that crystallize early in the reaction series at relatively high temperatures. Instead, thorium is incorporated into felsic minerals, which are the last to crystallize when magma cools and which largely make up continental crust. The earlier crystallization of mafic and intermediate minerals progressively enriches the remaining magma in incompatible elements such as Th, explaining the large difference in concentration between upper continental crust and basaltic oceanic crust. In open ocean sediments, away from fluvial, hemipelagic, and glaciogenic inputs of continental material, any appreciable amounts of Th are therefore thought to have been delivered by an eolian pathway.

An implicit assumption underlying this approach is that thorium concentrations in upper continental crust, and materials derived from it such as mineral dust, are invariant and close to 10.7 ppm. This assumption has been largely confirmed in a compilation of various geologic materials < 63 μm (McGee et al., 2007). More recently, however, McGee et al. (2016) showed a systematic increase in Th concentrations with decreasing grain-size in sediments from major dust source areas in East Asia, Australia and central South America. In the <5 μm size range, the average Th concentration in these materials is 14 ± 1 ppm (Fig. 1, *red line*), and this value is now recommended to estimate dust fluxes based on ^{232}Th where dust inputs are likely to be fine grained (McGee et al., 2016). The enrichment in fine size classes observed by McGee et al. (2016) is qualitatively supported by earlier Th measurements of global suspended (i.e., fine) river particulates in 10 of the world's largest river systems (14 ppm on average, Martin and Meybeck, 1979, Fig. 1). Similarly, analysis of fine African dust collected on Barbados (13.7 ± 1.2 ppm, Muhs et al. 2007), sediment from the Bodélé Depression in Chad (13 ± 1.3 ppm, Castillo et al., 2008) and surface soil from the western Sahara (13 ± 1 .3 ppm, Castillo et al., 2008) show Th concentrations close to 14 ppm (Fig.1, SPM dataset 1).

Some regional differences in dust composition, however, do exist (Fig.1). In fine dust (<3 μm) from the Hoggar region in Algeria, Th concentration is 17 ± 1.7 ppm and reflects the more felsic and geochemically evolved nature of the igneous and metamorphic bedrock in the region (Castillo et al. 2008; Moreno et al., 2006). Dust samples (<5 μm) from several coastal locations in Patagonia show Th concentrations close ~ 9.4 ± 1.7 ppm, likely due to presence of basaltic to basaltic-andesitic volcanic bedrock (McGee et al. 2016, Gaiero et al. 2007).

On regional scales, the exact concentration of Th in mineral dust will depend on the bedrock geology, weathering history of the source region, the transport history and dust grain-size (Moreno et al., 2006; Castillo et al., 2008, McGee et al. 2016). Acknowledging this caveat, the basic observation that ^{232}Th is significantly enriched in continental vs ocean crust remains valid and enables the use of ^{232}Th as tracer of continental and dust input to the ocean. Given that atmospheric dust transported over long distances typically displays a fine and well-sorted grain-size distribution (2-5 μm, e.g., Prospero and Bonatti, 1969, Mahowald et al. 2014, and references therein) we use 14 ppm instead of 10.7 ppm here as average ^{232}Th concentration in fine-grained continental material to quantify dust fluxes to the ocean.

The largest source of error in reconstructing dust flux using ^{232}Th in sediments is contamination by continental material of non-eolian origin, such as ice-rafted debris and hemipelagic material (i.e., terrestrial sediment that escaped the continental shelves). We systematically screen for these two sources of error by applying filters for latitude and distance offshore (section 3). Another potential bias is input of distal volcanic ash from regions of continental arc volcanism. For example, Quaternary ash tuff deposits in the northern Andes have relatively high Th concentrations (7.1 ppm ± 4.5ppm, n=6, Lebti et al., 2006) and could lead to overestimating dust in the Eastern Equatorial Pacific. The delivery of ^{232}Th from continents leads to measurable concentrations (~pg/kg) of dissolved ^{232}Th ($^{232}Th_{diss}$) in seawater, which are increasingly used to quantify present day dust deposition (Hsieh et al. 2011; Hayes et al. 2013; Lopez et al., 2015). The estimated fraction of dust-derived thorium that dissolves in seawater ranges from 1% to 20% (Hsieh et al., 2011; Hayes et al., 2013), and re-absorption of $^{232}Th_{diss}$ onto sinking particulates could lead to biases in low sedimentation rate regimes such as ocean gyres. Lastly, horizontal advection of fine particles by ocean surface currents can introduce uncertainties (Siegel and Deuser, 1997, Bory et al. 2002, Han et al., 2008), especially in fast flowing boundary currents (Rühleman and Butzin, 2006, van Sebille et al., 2015).

3 Methods and Approach

3.1 Assembly of the Database

We compiled ^{232}Th, ^{230}Th, and ^{238}U data and, if available ^{234}U sedimentary concentrations from the literature and from unpublished sources. We correct all ^{230}Th data for detrital and authigenic contributions and for decay since deposition based on established methods (Henderson and Anderson, 2003; François et al., 2004) and using the most recent half-life of ^{230}Th (75,548 ± 110 years; Cheng et al., 2013). Corrections for detrital ^{230}Th were applied using ^{238}U/^{232}Th activity ratios suggested for the Atlantic (0.6), Pacific (0.7) and Southern Ocean (0.4) following Henderson and Anderson (2003). For the Arabian Sea, 0.6 was used. We adopt core chronologies from the original publications, and we include U/Th datasets here that have not been used as dust indicators in their original contexts. References to the original studies are given in the supplementary material. We multiply the ^{230}Th-normalized bulk flux with the concentration of ^{232}Th to derive normalized ^{232}Th-fluxes with an average uncertainty (2-sigma) of 10%. The above approch is taken for all datasets with two exceptions. In two recent studies from the subarctic North Pacifc (Serno et al. 2014) and off subtropical Africa (McGee et al. 2013), geochemical and grainsize corrections were

applied to the ^{232}Th data to derive a refined estimate of dust deposition (*see below*). In these cases, we do not perform any re-calculations here but take the dust fluxes directly from the original studies

3.2 Description of the Full Database

The database contains records (n>300) from all major ocean basins, and includes sites from polar, temperate, and tropical regions. However, not all sites are suitable for dust reconstructions, as marine sediments typically are mixtures of various components. The lithogenic component, which includes not only continental dust, but also ice rafted debris and hemipelagic material (i.e., terrestrial sediment that escaped the continental shelves), forms the largest sediment input term to the ocean (20 Gigatons/yr), followed by biogenic debris (2 Gigatons/yr), volcanic ash, authigenic minerals, and meteoritic debris. Reliable dust reconstructions based on marine sediment cores therefore require careful site selection (Kohfeld and Harrison, 2001). We do not expect meteoritic and authigenic inputs to bias our ^{232}Th-based dust estimates due to their negligible overall magnitude. The largest potential bias to our estimates comes from hemipelagic and ice rafted contributions, both of which deliver significant amounts of continental ^{232}Th that is not associated with dust.

3.3 Screening of the Database

3.3.1. Identifying Hemipelagic Sites

Figures 2a and 3a show late Holocene (0-4 ka) Th-normalized ^{232}Th fluxes for all sites plotted against distance offshore and latitude, respectively. Many high values are found within 300 km off the coast, where fluvial and hemipelagic inputs are likely to be important. Beyond 300 km from the coast, most sites of non-polar origin (Fig. 2a, *black and red symbols*) have ^{232}Th values <200 µg/m^{2}yr and the values further decrease with increasing distance offshore. Similar to our findings, Singh et al. (2011) observed that Holocene ^{232}Th fluxes drop off precipitously with increasing distance from shore in the Eastern Equatorial Pacific (EEP). In order to avoid hemipelagic contributions, we categorically exclude all core sites that are within 300 km from the coast prior to reconstructing dust fluxes. Given significant fluvial inputs of the Amazon River (e.g., François and Bacon, 1991), the cut-off is 600 km and 800 km during the 0-4 ka and 19-23 ka time slice, respectively, in the western tropical Atlantic. Off subtropical Africa, however, McGee et al. (2013) combined grain-size end-member modeling and ^{230}Th-normalized bulk fluxes to correct for fluvial/hemipelagic inputs and to isolate the eolian signal in a set of cores that cover the last 20 ka. The 300 km offshore criterion is thus not applied in this data set (Fig. 2a, b, *red symbols*). A second data set in which corrections have been applied is from Serno et al. (2014), who used ^{4}He and ^{232}Th measurements in fine (<8 um) Asian dust source samples and a mixing model to isolate the eolian ^{232}Th component in a large set of core top samples from the subarctic North Pacific (Fig. 2a, b, *red symbols).*

3.3.2. Identifying Ice Rafted Sites

A steep poleward increase in fluxes is evident between 55-70°N and S in the un-screened database (Fig.3a), likely as result of ice rafting around the Arctic and Antarctic

continental margins. Under modern conditions, large tabular icebergs originating from the Antarctic Ice sheet initially accumulate in the Weddell Sea and then travel northwards until approximately 60°S, where they are swept into the eastward flowing Antarctic Circumpolar Current (ACC; Stuart and Long, 2011). Most icebergs have broken up by the time they reach the ACC (ibid) and are thus unlikely to occur in large numbers north of 50°S. To avoid ice rafted debris, we categorically exclude all sites more polar than 50° prior to reconstructing dust fluxes in the Southern Ocean and North Atlantic. Given the absence of a large continental ice sheet, the cut-off is only 55° in the North Pacific. We apply the same cut-off in the glacial time slice (19-23 ka, SPM Figs. S1 and S2), even though there is paleo-evidence that the Antarctic Polar Front (PF) may have shifted northward by 3-5° latitude (Kohfeld et al., 2013, Kanfoush et al. 2000). Nevertheless, the glacial database does not show a steep increase between 55 and 70°N and S, possibly because it contains much fewer sites. Acknowledging that the cut-offs used here are fixed in space and time, and thus static with climate, we think that the lack of direct observational constraints, including from particle size distributions and source fingerprinting, renders the isolation of IRD inputs at all sites hard to conclusively evaluate at this time.

In addition to the latitudinal and distance-offshore filters, we also screen out sites that are known drift deposits, those without chronological control, and sites affected by fluvial inputs even though they are beyond 300 km offshore. Figures 2b and 3b display ^{232}Th fluxes in the 0-4 ka time slice for the screened database versus distance offshore and latitude, respectively (see SPM Figs. S1 and S2 for 19-23 ka time slice).

3.3.3. Dust Deposition in ThoroMap

In the following, we use the screened database to derive dust deposition by dividing ^{230}Th-normalized fluxes of ^{232}Th by 14 ppm and refer to it as ThoroMap. The average analytical error of ^{232}Th-fluxes (±10%) and the reported uncertainty around the fine-grained crustal average (± 1 ppm; McGee et al., 2016) would result in a combined error of 12%. However, acknowledging regional differences in ^{232}Th concentration of fine-grained material, we take the difference between the recommended global value (14 ppm) and the Patagonian average (9.4 pm) to derive an uncertainty of ± 4.6 ppm around the fine-grained crustal average. This leads to a more conservative combined error of ±35%. The quantification of other potential sources of error, such as surface advection of suspended particles, is beyond the scope of the present study, but could be investigated using circulation models in the future (e.g., Rühleman and Buztin, 2006; van Sebille et al., 2015).

ThoroMap contains 157 and 76 sites in the 0-4 ka and 19-23 ka time slice, respectively. References to the original data sources are given in SPM datasets 2 and 3.

3.4 Models used

ThoroMap is compared with output from two numerical models. The most recent one is the Community Atmosphere Model version 4 (CAM4, Albani et al., 2014), which is part of the new Community Climate System model CCSM4. CCSM4 and its predecessor CCSM3 (Mahowald et al., 2006) are coupled atmosphere, land, ocean and sea ice models used for climate change scenarios (e.g., Hurrell et al., 2013). In CCSM3, Mahowald et al. (2006)

introduced a mineral aerosol source and deposition algorithm (Zender et al., 2003) to parameterize the sources, transport and deposition of mineral dust. Sources of dust were assumed to be dry, unvegetated regions with strong winds. Deposition processes include dry gravitational settling, turbulent dry deposition, and wet deposition during precipitation. The source and deposition schemes were slightly modified between CAM3 and CAM4, mostly due to a shift in the assumed size distribution to larger sizes (Albani et al., 2014; following Kok, 2011). Also, wet deposition in CAM4 was changed by increasing the solubility for dust particles and by using a larger below cloud scavenging coefficient for larger particles. Note that for CCSM4, we specifically use a 2 ka simulation (C4fn_2k, Albani et al., 2015) to make comparisons with the 0-4 ka time slice presented here. For CCSM3, no 2 ka simulation is available and we use the simulation for the current climate (CCSM3 SMOB, Mahowald et al., 2006). Both CCSM4 and CCSM3 have published simulations for the LGM, which are used here to make comparisons with the 19-23 ka ThoroMap time slice.

ThoroMap includes a limited number of sites that are also contained in the original datasets used to tune CCSM3 (DIRTMAP, Kohfeld and Harrison, 2001) and CCSM4 (Albani et al., 2014, SPM Table S3, Albani et al. 2015, Table 1), respectively. We exclude all of them prior to calculating correlation factors between models and Th-based dust (Figs.7, 8, Table 1), irrespective of the methods used to derive dust fluxes in the original publications.

4 Dust Reconstructions based on ThoroMap

4.1 The late Holocene time-slice

In the late Holocene, Th-based dust fluxes (n=157) range from roughly 0.1 to 17.7 g/m^{2}yr (Fig. 4a). Minimum deposition rates are observed in the eastern and western equatorial Pacific (EEP and WEP, respectively) and the Pacific sector of the Southern Ocean. Thorium based dust fluxes are maximal off northwest Africa, consistent with the proximity of this region to the Sahara-Sahel dust corridor. Relatively high values are also found at one site off Florida (9.7 g/m^{2}yr). 1987). It is surprising to only have a slightly lower deposition flux ~500 km off Florida compared to Africa, as changes in dust size distribution indicate scavenging (i.e., dry or wet deposition; Maring et al., 2003; Mahowald et al., 2014) and dust deposition in Miami, Florida was 1.6 g/m^{2}yr (1982-1983; Prospero et al., 1987). Possible explanations include that (a) there are significant variations of the seasonal positioning of the African dust plumes or (b) that this feature results from the vertical level of dust transport and the different scavenging mechanisms close to the African coast (prevalently dry) compared to the Caribbean (prevalently wet). Alternatively, the site off Florida could be biased by sediment redistribution in the strong nepheloid layer observed in this region (McCave 1986), which may have biased the deposition flux despite Th-normalization. Unfortunately, current lack of detailed observations (including on dust size and scavenging) prevents reaching any firm conclusion on this aspect.

Deposition rates are moderately high in the subarctic North Pacific (1-4 g/m^{2}yr) and in the tropical Atlantic off Brazil (4-6 g/m^{2}yr). ThoroMap also suggests moderately high deposition rates in the Atlantic sector of the Southern Ocean, where dust deposition decreases from 2-6 g/m^2 yr off Argentina to 0.5-2 g/m^{2}yr further east. All sites are north of the Polar Front, rendering ice rafted inputs unlikely.

4.2 The 19-23 ka time-slice

During the LGM, Th-based dust deposition rates (n=76) range from 0.1 to 29 g/m^{2}yr (Fig. 4b). Dust fluxes are higher than during the late Holocene at all sites, except off subtropical northwest Africa (Fig. 4c). Sites in the North Atlantic show deposition rates between 10-29 g/m^{2}yr, a 2-3 fold increase over late Holocene rates. Dust deposition is also strongly increased in the subarctic North Pacific and in the Atlantic sector of the Southern Ocean. In the EEP and WEP, glacial dust fluxes are consistently 2-3 times higher than late Holocene ones. Averaging from 0-7 ka instead of 0-4 ka, there is a 2-3 fold glacial increase in dust deposition supported by additional sites in the Indian Sector of the Southern Ocean (*not shown*).

ThoroMap shows increased dust deposition during the LGM compared to the late Holocene in all three of the modern HNLC regions, i.e., the Southern Ocean, the subarctic Pacific and the EEP. Earlier studies using age-model based mass accumulation rates of operationally defined eolian material found increased dust deposition during interglacials in the EEP (Rea, 1994; Murray et al., 1995). However, more recent studies using Th-normalized fluxes of ^{232}Th show that dust deposition was enhanced during glacials in the EEP and WEP (Anderson et al., 2006, McGee et al. 2007, Winckler et al., 2008; Kienast et al., 2013, Winckler et al. 2016, Costa et al., 2016). Based on a significant number of additional sites, ThoroMap supports these findings.

4.3 Comparison to other Datasets

DIRTMAP is an earlier global compilation of dust fluxes based on terrestrial loess deposits, ice cores, marine sediment traps and marine cores (Kohfeld and Harrison 2001, Kohfeld 2002, Maher et al., 2010). In Figure 5, we compare ThoroMap (*top*) with Holocene dust flux estimates from DIRTMAP-2 (*middle*). While the number and locations of sites are different in the two datasets, which makes direct comparisons difficult, the two datasets compare favorably overall. This is particularly true for the equatorial regions. However, ThoroMap differs from earlier dust flux reconstructions based on marine sediment cores, such as those compiled in DIRTMAP, in two key aspects. The earlier compilations are based on accumulation rates of the eolian fraction in sediments, where a) accumulation rate is the product of the age-model based linear sediment rate and dry bulk density (std error ±10-25%) and b) the eolian fraction is typically only operationally defined. This means that the sediment is subjected to various chemical leaching steps to isolate a crystalline, inorganic residue that is assumed to be eolian. The standard error with estimating the eolian fraction in this way is reported as ±10-40% in DIRTMAP (Kohfeld 2002). In this approach, the eolian fraction cannot be distinguished from other lithogenic fractions such as volcanic ash or ice rafted debris (Olivarez et al., 1991, Serno et al. 2014), which can lead to erroneously high estimates. Furthermore, it is now well recognized that age-model based accumulation rates cannot distinguish between laterally advected particle fluxes and vertical particle fluxes from the sea surface, which are the variable of interest (e.g., François et al. 2004, 2007; Kienast et al. 2007, Marcantonio et al. 2014). ThoroMap makes use of the increased availability of ICP-MS measurements of Th and U isotopes and thus offers two important advantages. The eolian fraction is measured more directly with ^{232}Th, and flux estimates based on ^{230}Th-normalization are significantly less likely to be biased by local-scale syndepositional sediment redistribution on the sea floor compared to traditional age-model based chronologies. Thorium-normalization also reduces sensitivity to age-model errors.

Recently, Albani et al. (2014) compiled modern dust flux observations from atmospheric sampling, ice cores, and sediment traps and included an estimate of the <10 μm fraction (Fig. 5, *bottom*). This dataset also compares well with ThoroMap, in particular in the WEP and off northwest Africa. Note that the dust values observed off Argentina (2-6 g/m^{2}yr) in ThoroMap (Figure 5a) fall on a gradient between values of >20 g/m^{2}yr in continental Argentina and <0.1 g/m^{2}yr on James Ross Island, Antarctica (Figure 5c)**.**

4.4 Comparison between ThoroMap and Models

In an ideal comparison between geological observations and models, particle size ranges would coincide. While CCSM4 simulates dust diameters ≤ 10 μm, ThoroMap does not presently include specific size information. Given that the inverse relationship between grain size and distance from source area is widely recognized (Albani et al., 2015; Lawrence and Neff, 2009; Pye 1995, Prospero and Bonatti, 1969), we assume here that dust reaching screened sites in ThoroMap is predominately fine (<10 μm) and that the following comparisons are robust.

4.4.1 Late Holocene

ThoroMap offers insight in areas such as the Atlantic sector of the Southern Ocean and the EEP, which are not well represented in current observational databases (Fig.5). After excluding any sites that have been used in the calibration of the models (*section 3.5*), we directly compare the model output with ThoroMap (Fig. 7,8). The range in absolute dust values (0-4 ka) is remarkably similar between ThoroMap (0.08-9.73 g/m^2yr, n=135) and CCSM4 (0.02-7.96 g/m^2yr). Model-data agreement is within a factor of ten at many sites with a statistical correlation of 0.63 for CCSM3 and 0.59 for CCSM4 (Table 1) in the late Holocene time slice.

At none of the sites do the models overestimate dust deposition by a factor of ten; however, they underestimate it by a factor of ten or more in some locations in comparison to ThoroMap. The number of apparently underestimated sites in CCSM4 is greater than in CCSM3 (Fig. 7). CCSM4 predicts lower late Holocene dust deposition in comparison to ThoroMap chiefly in the Atlantic Sector of the Southern Ocean (off Argentina) and the mid-latitude South Atlantic (Fig. 6; 7a, *light blue circles, open purple squares*). Interestingly, the agreement between ThoroMap and the earlier CCSM3 model is much higher in these two regions (Fig. 7b). In addition, CCSM4 as well as CCSM3 predict much lower dust fluxes than ThoroMap in the western equatorial Pacific (Fig. 6; Fig.7a,b, *solid red squares*).

ThoroMap sites in the Atlantic sector of the Southern Ocean could, in principle, be contaminated by unrecognized ice-rafted inputs north of the Polar Front, although we consider systematic contamination by ice rafted debris unlikely north of 50°S (*section 2*). Note that using ~ 9.4 instead of 14 ppm as a regional crustal Th-concentration for South-America (*section 2*) would make the Th-based dust estimates even higher in this region. This area is subject to strong bottom currents (McCave 1986), which could potentially lead to errors in estimating sedimentary fluxes even when using Th-normalization. However, the model-data agreement in this region is much better for CCSM3, consistent with the difficulty of the CCSM4 model to obtain realistic dust sources in South America without tuning (Albani et al., 2014). Also, observed modern dust deposition is high in Argentina (>20 g/m^2yr, Fig.5, *bottom*), in line with ThoroMap estimates offshore of South America. A 6 ka simulation (Albani et al., 2015) is in better agreement with the late Holocene time slice in ThoroMap in the Atlantic sector of the Southern Ocean, suggesting that some of the discrepancy between CCSM4 and ThoroMap could be related to the choice of time interval.

In the subarctic and mid-latitude Pacific, the match between both models and ThoroMap is good (Fig.6; Fig.7 a, b, *dark blue and green squares and circles*). Similarly, the correlation between both models, in particular CCSM4, and ThoroMap is strong in the EEP (Fig.6, Fig. 7 a, b, *red circles*). However, both models appear to underestimate dust deposition in the WEP, CCSM4 even more so than CCSM3 (Fig. 7a,b; *red squares*). An earlier, composite model (Mahowald et al. 2005; *not shown*) predicts deposition rates of ~0.1-0.5 g/m^2yr in the western equatorial Pacific and would thus fit better with ThoroMap in this region. This observation, in agreement with Winckler et al. (2008), suggests that dust sources may be underestimated in the WEP by both CCSM4 and CCSM3.

4.4.2. 19-23 ka time-slice

The statistical correlation between ThoroMap and models is high for the 19-23 ka time slice, with a spearman's rho of 0.83 for CCSM4 (n=54) and 0.82 for CCSM3 (n=67 ; Table 1). The WEP is the only region where both models underestimate dust flux by a factor of ten compared to ThoroMap (Fig. 8a,b; *solid red squares*).

5 Conclusions

We compiled published ^{232}Th, ^{230}Th, and ^{238}U data and chronological information from marine sediment cores to build ThoroMap, a new global database of marine dust deposition records for the late Holocene (0-4 ka) and the LGM (19-23 ka). ThoroMap is compared to output from two recent coupled climate models, CCSM3 and CCSM4. Key findings are as follows:

1) Th-based dust fluxes range from 0.1-17.7 g/m^{2}yr during the late Holocene (n=157) with minimal deposition in the EEP, WEP, and the Pacific sector of the Southern Ocean. Maximum dust fluxes are observed off northwest Africa, consistent with the proximity of this region to the Sahara-Sahel dust source region.

2) As in previous studies, late Holocene dust fluxes are significantly lower than LGM fluxes, which range from 0.1 to 29 g/m^{2}yr (n=76). The only exception is off northwest Africa, downstream of the Sahara-Sahel dust corridor, where glacial and late Holocene dust fluxes are not significantly different.

3) Th-based dust deposition in the WEP is significantly higher than predicted by both CCSM3 and CCSM4 in the late Holocene as well as the LGM.

4) The observed match between CCSM4 and ThoroMap is good in the EEP, the subarctic and mid-latitude Pacific, and off northwest Africa in the late Holocene. CCSM3 agrees with ThoroMap in these regions as well as in the Atlantic Sector of the Southern Ocean. In the 0-4 ka time slice, data-model correlation factors are 0.59 and 0.63 for CCSM4 (n=135) and CCSM3 (n=148) , respectively. In the LGM time slice, the match between models and Thoromap is 0.82 (CCSM4, n=54) and 0.83 (CCSM3, n=67) . All sites included in these correlations have not been used previously to tune the models.

5) ThoroMap builds on DIRTMAP, an earlier widely used global compilation of dust deposition. Making use of the increased availability of ICP-MS measurements, ThoroMap exclusively uses ^{230}Th-normalized fluxes of the continental isotope ^{232}Th to estimate dust deposition, with an estimated uncertainy of 35 %. Thus, ThoroMap is able to refine DIRTMAP in two important aspects. The eolian fraction is measured more directly with ^{232}Th, and accumulation is more accurately estimated by ^{230}Th normalization.

Acknowledgments

We greatly acknowledge official reviews by David McGee and one anonymous reviewer, which improved the manuscript, and fruitful discussions with Karen Kohfeld, Dan Kelley, Anne Marie Ryan, and Bob Anderson. Roger François and Samuel Jaccard generously shared unpublished data. S.K. was supported by grants from the National Science and Engineering Council Canada (NSERC). J.L. was supported by the FP7-PEOPLE-2013-IEF, Marie Curie proposal 622483. G.W., N.M. and S.A. were supported by the US National Science Foundation, through grants AGS-1003505 and 1003509. ThoroMap contributes to the goals of the Past Global Changes (PAGES) working group DICE (Dust Impacts on Climate and Environment) and will be made available as supplementary material to this article and at NOAA NCEI, https://www.ncdc.noaa.gov/data-access/paleoclimatology-data.

References

Adkins, J., deMenocal, P., & Eshel, G. (2006). The "African humid period" and the record of marine upwelling from excess Th-230 in Ocean Drilling Program Hole 658C. Paleoceanography, 21(4). doi:Pa420310.1029/2005pa001200

Albani, S., Mahowald, N. M., Perry, A. T., Scanza, R. A., Zender, C. S., Heavens, N. G., . . . Otto-Bliesner, B. L. (2014). Improved dust representation in the Community Atmosphere Model. Journal of Advances in Modeling Earth Systems, 6(3), 541-570. doi:10.1002/2013ms000279

Albani, S., Mahowald, N. M., Winckler, G., Anderson, R. F., Bradtmiller, L. I., Delmonte, B., . . . Sun, J. (2015). Twelve thousand years of dust: the Holocene global dust cycle constrained by natural archives. Climate of the Past, 11(6), 869-903. doi:10.5194/cp-11-869-2015

Anderson, R. F., Fleischer, M. Q., & Lao, Y. (2006). Glacial-interglacial variability in the delivery of dust to the central equatorial Pacific. Earth and Planetary Science Letters, 242, 406-414.

Atkinson, J. D., Murray, B. J., Woodhouse, M. T., Whale, T. F., Baustian, K. J., Carslaw, K. S., . . . Malkin, T. L. (2013). The importance of feldspar for ice nucleation by mineral dust in mixed-phase clouds. Nature, 498(7454), 355-358. doi:10.1038/nature12278

Bacon, M. P. (1984). Glacial to interglacial changes in carbonate and clay sedimentation in the Atlantic Ocean estimated from 230 Th measurements. Isotope Geoscience, 2, 97-111.

Booth, B. B. B., Dunstone, N. J., Halloran, P. R., Andrews, T., & Bellouin, N. (2012). Aerosols implicated as a prime driver of twentieth-century North Atlantic climate variability. Nature, 484(7393), 228-U110. doi:10.1038/nature10946

Bory, A., Dulac, F., Moulin, C., Chiapello, I., Newton, P. P., Guelle, W., . . . Bergametti, G. (2002). Atmospheric and oceanic dust fluxes in the northeastern tropical Atlantic Ocean: how close a coupling? Annales Geophysicae, 20(12), 2067-2076.

Boucher, O., Randall, D., Artaxo, P., Bretherton, C., Feingold, G., Forster, P., . . . Zhang, X. Y. (2013). Clouds and Aerosols. In T. F. Stocker, D. Qin, G.-K. Plattner, M. Tignor, S. K. Allen, J. Boschung, A. Nauels, Y. Xia, V. Bex, & P. M. Midgley (Eds.), Climate Change 2013: The Physical Science Basis. Contribution of Working Group I to the Fifth Assessment Report of the Intergovernmental Panel on Climate Change. Cambridge, United Kingdom and New York, NY, USA: Cambridge University Press.

Boyd, P. W., Jickells, T., Law, C. S., Blain, S., Boyle, E. A., Buesseler, K. O., . . . Watson, A. J. (2007). Mesoscale iron enrichment experiments 1993-2005: Synthesis and future directions. Science, 315(5812), 612-617. doi:10.1126/science.1131669

Bradtmiller, L. I., Anderson, R. F., Fleisher, M. Q., & Burckle, L. H. (2007). Opal burial in the equatorial Atlantic Ocean over the last 30 ka: Implications for glacial-interglacial changes in the ocean silicon cycle. Paleoceanography, 22. doi:10.1029/2007PA001443

Castillo, S., Moreno, T., Querol, X., Alastuey, A., Cuevas, E., Herrmann, L., . . . Gibbons, W. (2008). Trace element variation in size-fractionated African desert dusts. Journal of Arid Environments, 72(6), 1034-1045. doi:10.1016/j.jaridenv.2007.12.007

Cheng, H., Edwards, R. L., Shen, C.-C., Polyak, V. J., Asmerom, Y., Woodhead, J., . . . Alexander, E. C., Jr. (2013). Improvements in Th-230 dating, Th-230 and U-234 half-life values, and U-Th isotopic measurements by multi-collector inductively coupled plasma mass spectrometry. Earth and Planetary Science Letters, 371, 82-91. doi:10.1016/j.epsl.2013.04.006

Conway, H., Gades, A., & Raymond, C. F. (1996). Albedo of dirty snow during conditions of melt. Water Resources Research, 32(6), 1713-1718. doi:10.1029/96wr00712

Costa, K. M., McManus, J. F., Anderson, R. F., Ren, H., Sigman, D. M., Winckler, G., . . . Ravelo, A. C. (2016). No iron fertilization in the equatorial Pacific Ocean during the last ice age. Nature, 529, 519-522. doi:doi:10.1038/nature16453

Francois, R., Frank, M., Loeff, M. M. R. v. d., & Bacon, M. P. (2004). 230Th normalization: An essential tool for interpreting sedimentary fluxes during the late Quaternary. Paleoceanography, 19. doi:10.1029/2003PA000939

Francois, R., Frank, M., Loeff, M. R. v. d., Bacon, M. P., Geibert, W., Kienast, S., . . . Allen, S. E. (2007). Comment on " Do geochemical estimates of sediment focusing pass the sediment test in the equatorial Pacific" by Lyle et al. Paleoceanography, 22. doi:10.1029/2005PA001235

Ginoux, P., Prospero, J. M., Gill, T. E., Hsu, N. C., & Zhao, M. (2012). Global-scale attribution of anthropogenic and natural dust sources and their emission rates based on MODIS DEEP BLUE aerosols products. *Reviews of Geophysics, 50*. doi:10.1029/2012rg000388

Han, Q., Moore, J. K., Zender, C., Measures, C., & Hydes, D. (2008). Constraining oceanic dust deposition using surface ocean dissolved Al. Global Biogeochemical Cycles, 22(2). doi:10.1029/2007gb002975

Hayes, C. T., Anderson, R. F., Fleisher, M. Q., Serno, S., Winckler, G., & Gersonde, R. (2013). Quantifying lithogenic inputs to the North Pacific Ocean using the long-lived thorium isotopes. *Earth and Planetary Science Letters, 383*, 16-25. doi:10.1016/j.epsl.2013.09.025

Henderson, G. M., & Anderson, R. F. (2003). The U-series toolbox for paleoceanography. Uranium-Series Geochemistry, 52, 493-531. doi:10.2113/0520493

Hsieh, Y.-T., Henderson, G. M., & Thomas, A. L. (2011). Combining seawater Th-232 and Th-230 concentrations to determine dust fluxes to the surface ocean. *Earth and Planetary Science Letters, 312*(3-4), 280-290. doi:10.1016/j.epsl.2011.10.022

Hurrell, J. W., Holland, M. M., Gent, P. R., Ghan, S., Kay, J. E., Kushner, P. J., . . . Marshall, S. (2013). The Community Earth System Model A Framework for Collaborative Research. Bulletin of the American Meteorological Society, 94(9), 1339-1360. doi:10.1175/bams-d-12-00121.1

Jaccard, S. L., Hayes, C. T., Martinez-Garcia, A., Hodell, D. A., Anderson, R. F., Sigman, D. M., & Haug, G. H. (2013). Two Modes of Change in Southern Ocean Productivity Over the Past Million Years. Science, 339(6126), 1419-1423. doi:10.1126/science.1227545

Jacobel, A. W., McManus, J. F., Anderson, R. F., & Winckler, G. (2016). Large deglacial shifts of the Pacific Intertropical Convergence Zone. Nature communications, 7, 10449-10449. doi:10.1038/ncomms10449

Kanfoush, S. L., Hodell, D. A., Charles, C. D., Guilderson, T. P., Mortyn, P. G., & Ninnemann, U. S. (2000). Millennial-scale instability of the antarctic ice sheet during the last glaciation. Science, 288(5472), 1815-1818. doi:10.1126/science.288.5472.1815

Kienast, S. S., M. Kienast, A. C. Mix, S. E Calvert, and R. François. (2007). Thorium-230 normalized particle flux and sediment focusing in the Panama Basin region during the last 30,000 years. Paleoceanography, 22. doi:10.1029/2006PA001357, 2007

Kienast, S. S., Friedrich, T., Dubois, N., Hill, P. S., Timmermann, A., Mix, A. C., & Kienast, M. (2013). Near collapse of the meridional SST gradient in the eastern equatorial Pacific during Heinrich Stadial 1. Paleoceanography, 28. doi:doi:10.1002/2013PA002499

Kohfeld, K. E. (2002). DIRTMAP Version 2. LGM and Late Holocene Eolian Fluxes from Ice Cores, Marine Sediment Traps, Marine Sediments, and Loess DepositsGBP PAGES/World Data Center for Paleoclimatology NOAA/NGDC Paleoclimatology Program, Boulder CO, USA, Data Contribution Series #2002-045. .

Kohfeld, K. E., Graham, R. M., de Boer, A. M., Sime, L. C., Wolff, E. W., Le Quere, C., & Bopp, L. (2013). Southern Hemisphere westerly wind changes during the Last Glacial Maximum: paleo-data synthesis. Quaternary Science Reviews, 68, 76-95. doi:10.1016/j.quascirev.2013.01.017

Kohfeld, K. E., & Harrison, S. P. (2001). DIRTMAP: The geological record of dust. Earth Science Reviews, 54, 81-114.

Kok, J. F. (2011). A scaling theory for the size distribution of emitted dust aerosols suggests climate models underestimate the size of the global dust cycle. Proceedings of the National Academy of Sciences of the United States of America, 108(3), 1016-1021. doi:10.1073/pnas.1014798108

Lamy, F., Gersonde, R., Winckler, G., Esper, O., Jaeschke, A., Kuhn, G., . . . Kilian, R. (2014). Increased Dust Deposition in the Pacific Southern Ocean During Glacial Periods. Science, 343(6169), 403-407. doi:10.1126/science.1245424

Lawrence, C. R., & Neff, J. C. (2009). The contemporary physical and chemical flux of aeolian dust: A synthesis of direct measurements of dust deposition. Chemical Geology, 267(1-2), 46-63. doi:10.1016/j.chemgeo.2009.02.005

Lebti, P. P., Thouret, J. C., Worner, G., & Fornari, M. (2006). Neogene and Quaternary ignimbrites in the area of Arequipa, Southern Peru: Stratigraphical and petrological correlations. *Journal of Volcanology and Geothermal Research, 154*(3-4), 251-275. doi:10.1016/j.jvolgeores.2006.02.014

Lopez, G. I., Marcantonio, F., Lyle, M., & Lynch-Stieglitz, J. (2015). Dissolved and particulate Th-230-Th-232 in the Central Equatorial Pacific Ocean: Evidence for far-field transport of the East Pacific Rise hydrothermal plume. *Earth and Planetary Science Letters, 431*, 87-95. doi:10.1016/j.epsl.2015.09.019

Maher, B. A., Prospero, J. M., Mackie, D., Gaiero, D., Hesse, P. P., & Balkanski, Y. (2010). Global connections between aeolian dust, climate and ocean biogeochemistry at the present day and at the last glacial maximum. Earth-Science Reviews, 99(1-2), 61-97. doi:10.1016/j.earscirev.2009.12.001

Mahowald, N., Albani, S., Kok, J. F., Engelstaeder, S., Scanza, R., Ward, D. S., & Flanner, M. G. (2014). The size distribution of desert dust aerosols and its impact on the Earth system. Aeolian Research, 15, 53-71. doi:10.1016/j.aeolia.2013.09.002

Mahowald, N. M., Kloster, S., Engelstaedter, S., Moore, J. K., Mukhopadhyay, S., McConnell, J. R., . . . Zender, C. S. (2010). Observed 20th century desert dust variability: impact on climate and biogeochemistry. Atmospheric Chemistry and Physics, 10(22), 10875-10893. doi:10.5194/acp-10-10875-2010

Mahowald, N. M., Muhs, D. R., Levis, S., Rasch, P. J., Yoshioka, M., Zender, C. S., & Luo, C. (2006). Change in atmospheric mineral aerosols in response to climate: Last glacial period, preindustrial, modern, and doubled carbon dioxide climates. Journal of Geophysical Research-Atmospheres, 111(D10), 22. doi:D1020210.1029/2005jd006653

Mahowald, N. M., Baker, A. R., Bergametti, G., Brooks, N., Duce, R. A., Jickells, T. D., . . . Tegen, I. (2005). Atmospheric global dust cycle and iron inputs to the ocean. Global Biogeochemical Cycles, 19(4). doi:10.1029/2004gb002402

Marcantonio, F., Lyle, M., & Ibrahim, R. (2014). Particle sorting during sediment redistribution processes and the effect on 230Th-normalized mass accumulation rates. Geophysical Research Letters, - 41(- 15).

Maring, H., Savoie, D. L., Izaguirre, M. A., Custals, L., & Reid, J. S. (2003). Mineral dust aerosol size distribution change during atmospheric transport. Journal of Geophysical Research-Atmospheres, 108(D19). doi:10.1029/2002jd002536

Martinez-Garcia, A., Rosell-Mele, A., Geibert, W., Gersonde, R., Masque, P., Gaspari, V., & Barbante, C. (2009). Links between iron supply, marine productivity, sea surface temperature, and CO2 over the last 1.1 Ma. Paleoceanography, 24. doi:Pa1207 10.1029/2008pa001657

Martinez-Garcia, A., Rosell-Mele, A., Jaccard, S. L., Geibert, W., Sigman, D. M., & Haug, G. H. (2011). Southern Ocean dust-climate coupling over the past four million years. Nature, 476(7360), 312-U141. doi:10.1038/nature10310

McCave, I. N. (1986). Local and global aspects of the bottom nepheloid layers in the world ocean.

McGee, D., Winckler, G., Borunda, A., Serno, S., Anderson, R. F., Recasens, C., . . . Sun, Y. (2016). Tracking eolian dust with helium and thorium: Impacts of grain size and provenance. Geochimica Et Cosmochimica Acta, 175, 47-67.

McGee, D., deMenocal, P. B., Winckler, G., Stuut, J. B. W., & Bradtmiller, L. I. (2013). The magnitude, timing and abruptness of changes in North African dust deposition over the last 20,000 yr. Earth and Planetary Science Letters, 371, 163-176. doi:10.1016/j.epsl.2013.03.054

McGee, D., Marcantonio, F., McManus, J. F., & Winckler, G. (2010). The response of excess 230Th and extraterrestrial 3He to sediment redistribution at the Blake Ridge, western North Atlantic. Earth and Planetary Science Letters, 299, 138-149.

McGee, D., Marcantonio, F., & Lynch-Stieglitz, J. (2007). Deglacial changes in dust flux in the eastern equatorial Pacific. Earth and Planetary Science Letters, 257, 215-230.

Moreno, T., Querol, X., Castillo, S., Alastuey, A., Cuevas, E., Herrmann, L., . . . Gibbons, W. (2006). Geochemical variations in aeolian mineral particles from the Sahara-Sahel Dust Corridor. Chemosphere, 65(2), 261-270. doi:10.1016/j.chemosphere.2006.02.052

Muhs, D. R., Budahn, J. R., Prospero, J. M., & Carey, S. N. (2007). Geochemical evidence for African dust inputs to soils of western Atlantic islands: Barbados, the Bahamas, and Florida. *Journal of Geophysical Research-Earth Surface, 112*(F2). doi:10.1029/2005jf000445

Mulitza, S., Heslop, D., Pittauerova, D., Fischer, H. W., Meyer, I., Stuut, J.-B., . . . Schulz, M. (2010). Increase in African dust flux at the onset of commercial agriculture in the Sahel region. Nature, 466(7303), 226-228. doi:10.1038/nature09213

Murray, R. W., Leinen, M., Murray, D. W., Mix, A. C., & Knowlton, C. W. (1995). Terrigenous Fe input and biogenic sedimentation in the glacial and interglacial equatorial Pacific Ocean. Global Biogeochemical Cycles, 9(4), 667-684.

Olivarez, A. M., Owen, R. M., & Rea, D. K. (1991). GEOCHEMISTRY OF EOLIAN DUST IN PACIFIC PELAGIC SEDIMENTS - IMPLICATIONS FOR PALEOCLIMATIC INTERPRETATIONS. Geochimica Et Cosmochimica Acta, 55(8), 2147-2158. doi:10.1016/0016-7037(91)90093-k

Orsi, A. H., Whitworth, T., & Nowlin, W. D. (1995). ON THE MERIDIONAL EXTENT AND FRONTS OF THE ANTARCTIC CIRCUMPOLAR CURRENT. Deep-Sea Research Part I-Oceanographic Research Papers, 42(5), 641-673. doi:10.1016/0967-0637(95)00021

Pourmand, A., Marcantonio, F., & Schulz, H. (2004). Variations in productivity and eolian fluxes in the northeastern Arabian Sea during the past 110 ka. *Earth and Planetary Science Letters, 221*(1-4), 39-54. doi:10.1016/s0012-821x(04)00109-8

Prospero, J. M., & Bonatti, E. (1969). Continental Dust in the Atmosphere of the Eastern Equatorial Pacific. Jour. of Geophysical Res., 74(13), 3362-3371.

Prospero, J. M., Nees, R. T., & Uematsu, M. (1987). DEPOSITION RATE OF PARTICULATE AND DISSOLVED ALUMINUM DERIVED FROM SAHARAN DUST IN PRECIPITATION AT MIAMI, FLORIDA. *Journal of Geophysical Research-Atmospheres, 92*(D12), 14723-14731. doi:10.1029/JD092iD12p14723

Rea, D. K. (1994). The paleoclimatic record provided by eolian deposition in the deep sea: the geologic history of wind. Reviews of Geophysics, 32(2), 159-195.

Rudnick, R. L., & Gao, S. (2004). Composition of the Continental Crust. In H. D. Holland & K. K. Turekian (Eds.), *Treatise on Geochemistry* (Vol. 3, pp. 1-64). Amsterdam: Elsevier.

Rühlemann, C., & Butzin, M. (2006). Alkenone temperature anomalies in the Brazil-Malvinas Confluence area caused by lateral advection of suspended particulate material. *Geochemistry Geophysics Geosystems, 7*. doi:10.1029/2006gc001251

Schulz, M., Prospero, J. M., Baker, A. R., Dentener, F., Ickes, L., Liss, P. S., . . . Duce, R. A. (2012). Atmospheric Transport and Deposition of Mineral Dust to the Ocean: Implications for Research Needs. Environmental Science & Technology, 46(19), 10390-10404. doi:10.1021/es300073u

Serno, S., Winckler, G., Anderson, R. F., Hayes, C. T., McGee, D., Machalett, B., . . . Haug, G. H. (2014). Eolian dust input to the Subarctic North Pacific. Earth and Planetary Science Letters, 387, 252-263. doi:10.1016/j.epsl.2013.11.008

Siegel, D. A., & Deuser, W. G. (1997). Trajectories of sinking particles in the Sargasso Sea: modeling of statistical funnels above deep-ocean sediment traps. Deep-Sea Research Part I-Oceanographic Research Papers, 44(9-10), 1519-1541. doi:10.1016/s0967-0637(97)00028-9

Singh, A. K., Marcantonio, F., & Lyle, M. (2011). Sediment focusing in the Panama Basin, Eastern Equatorial Pacific. Earth and Planetary Science Letters, 309, 33-44.

Stuart, K. M., & Long, D. G. (2011). Tracking large tabular icebergs using the SeaWinds Ku-band microwave scatterometer. Deep-Sea Research Part Ii-Topical Studies in Oceanography, 58(11-12), 1285-1300. doi:10.1016/j.dsr2.2010.11.004

Taylor, S. R., & McClennan, S. M. (1985). The continental crust: its composition and evolution: Blackwell Scientific Publications.

van Sebille, E., Scussolini, P., Durgadoo, J. V., Peeters, F. J. C., Biastoch, A., Weijer, W., . . . Zahn, R. (2015). Ocean currents generate large footprints in marine palaeoclimate proxies. Nature communications, 6. doi:10.1038/ncomms7521

Ward, D. S., Mahowald, N. M., & Kloster, S. (2014). Potential climate forcing of land use and land cover change. Atmospheric Chemistry and Physics, 14(23), 12701-12724. doi:10.5194/acp-14-12701-2014

Werner, M., Tegen, I., Harrison, S. P., Kohfeld, K. E., Prentice, I. C., Balkanski, Y., . . . Roelandt, C. (2002). Seasonal and interannual variability of the mineral dust cycle under present and glacial climate conditions. Jour. of Geophysical Res., 107(D24, 4744), doi: 10.1029/2002JD002365.

Winckler, G., Anderson, R. F., Jaccard, S. L., & Marcantonio, F. (2016). Ocean dynamics, not dust, have controlled equatorial Pacific productivity over the past 500,000 years. *Proceedings of the National Academy of Sciences of the United States of America, 113*(22), 6119-6124. doi:10.1073/pnas.1600616113

Winckler, G., Anderson, R. F., Fleischer, M. Q., McGee, D., & Mahowald, N. (2008). Covariant Glacial-Interglacial dust fluxes in the Equatorial Pacific and Antarctica. Science, 320, 93-96.

Winckler, G., Anderson, R. F., & Schlosser, P. (2005). Equatorial Pacific productivity and dust flux during the mid-Pleistocene climate transition. Paleoceanography, 20(4), 10. doi:10.1029/2005pa001177

Woodard, S. C., Thomas, D. J., & Marcantonio, F. (2012). Thorium-derived dust fluxes to the tropical Pacific Ocean, 58 Ma. Geochimica Et Cosmochimica Acta, 87, 194-209. doi:10.1016/j.gca.2012.03.035

Zender, C., Bian, H., & Newman, D. (2003). Mineral Dust Entrainment and Deposition (DEAD) model: Description and 1990s dust climatology. Journal of Geopysical Research, 108(D14), 4461. doi:10.1029/2002JD002775

References for Datasets S2 and S3

Anderson, R. F., Fleischer, M. Q., & Lao, Y. (2006). Glacial-interglacial variability in the delivery of dust to the central equatorial Pacific. *Earth and Planetary Science Letters, 242*, 406-414.

Anderson, R. F., Ali, S., Bradtmiller, L. I., Nielsen, S. H. H., Fleisher, M. Q., Anderson, B. E., & Burckle, L. H. (2009). Wind-driven upwelling in the Southern Ocean and the deglacial rise in atmospheric CO2. Science, 323, 1443-1448.

Anderson, R. F., Barker, S., Fleisher, M., Gersonde, R., Goldstein, S. L., Kuhn, G., . . . Sachs, J. P. (2014). Biological response to millennial variability of dust and nutrient supply in the Subantarctic South Atlantic Ocean. Philosophical Transactions of the Royal Society A, 372 doi:10.1098/rsta.2013.0054

Benway, H. M., Mix, A. C., Haley, B. A., & Klinkhammer, G. P. (2006). Eastern Pacific Warm Pool paleosalinity and climate variability: 0-30 kyr. Paleoceanography, 21(3). doi:10.1029/2005pa001208

Bradtmiller, L. I., Anderson, R. F., Fleisher, M. Q., & Burckle, L. H. (2006). Diatom productivity in the Equatorial Pacific Ocean from the Last Glacial Maximum to the present: A test of the silicic acid leakage hypothesis. Paleoceanography, 21. doi:10.1029/2006PA001282

Bradtmiller, L. I., Anderson, R. F., Fleisher, M. Q., & Burckle, L. H. (2007). Opal burial in the equatorial Atlantic Ocean over the last 30 ka: Implications for glacial-interglacial changes in the ocean silicon cycle. Paleoceanography, 22. doi:10.1029/2007PA001443

Bradtmiller, L. I., Anderson, R. F., Fleisher, M. Q., & Burckle, L. H. (2009). Comparing glacial and Holocene opal fluxes in the Pacific sector of the Southern Ocean. Paleoceanography, 24. doi:10.1029/2008PA001693

Broecker, W. S., Oppo,D., Peng, T.-H., Curry, W. Andree, M., Wolfli, W., Bonani, G. (1988). Radiocarbon-based Chronology for the 18O/16O record for the last deglaciation. Paleoceanography, 3(4), 509-515.

Chapman, M. R., Shackleton, N. J., & Duplessy, J. C. (2000). Sea surface temperature variability during the last glacial-interglacial cycle: assessing the magnitude and pattern of climate change in the North Atlantic. Palaeogeography Palaeoclimatology Palaeoecology, 157(1-2), 1-25. doi:10.1016/s0031-0182(99)00168-6

Costa, K. M., McManus, J. F., Anderson, R. F., Ren, H., Sigman, D. M., Winckler, G., . . . Ravelo, A. C. (2016). No iron fertilization in the equatorial Pacific Ocean during the last ice age. *Nature, 529*, 519-522. doi:doi:10.1038/nature16453

Dezileau, L., Bareille, G., Reyss, J. L., & Lemoine, F. (2000). Evidence for strong sediment redistribution by bottom currents along the southeast Indian ridge. Deep-Sea Research Part I-Oceanographic Research Papers, 47(10), 1899-1936. doi:10.1016/s0967-0637(00)00008-x

Dubois, N., Kienast, M., Kienast, S., Normandeau, C., Calvert, S. E., Herbert, T. D., & Mix, A. (2011). Millennial-scale variations in hydrography and biogeochemistry in the Eastern Equatorial Pacific over the last 100 kyr. Quaternary Science Reviews, 30, 210-233.

Feldberg, M. J., & Mix, A. C. (2003). Pianktonic foraminifera, sea surface temperatures, and mechanisms of oceanic change in the Peru and south equatorial currents, 0-150 ka BP (DOI 10.1029/2001PA000740). Paleoceanography, 18(1), 16.

François, R., Bacon, M. P., & Suman, D. O. (1990). Thorium 230 profiling in deep sea sediments: High-resolution records of flux and dissolution of carbonate in the equatorial atlantic during the last 24,000 years. Paleoceanography, 5(5), 761-787.

Gottschalk, J., Skinner, L., Lippold, J., Vogel, H., N Frank, Jaccard, S., & Waelbroeck, C. (2016). Synergy of biological and physical controls in the Southern Ocean on past

millennial-scale atmospheric CO2 changes. Nature Communications, submitted.
Grousset, F. E., Labeyrie, L., Sinko, J. A., Cremer, M., Bond, G., Duprat, J., . . . Huon, S. (1993). Patterns of ice-rafted detritus in the glacial North-Atlantic (40 degrees-55-degrees N) Paleoceanography, 8(2), 175-192. doi:10.1029/92pa02923
Grutzner, J., Giosan, L., Franz, S. O., Tiedemann, R., Cortijo, E., Chaisson, W. P., . . . Williams, T. (2002). Astronomical age models for Pleistocene drift sediments from the western North Atlantic (ODP Sites 1055-1063). Marine Geology, 189(1-2), 5-23. doi:10.1016/s0025-3227(02)00320-1
Kienast, S. S., M. Kienast, A. C. Mix, S. E Calvert, and R. François. (2007). Thorium-230 normalized particle flux and sediment focusing in the Panama Basin region during the last 30,000 years. Paleoceanography, 22. doi:10.1029/2006PA001357, 2007
Koutavas, A., & Lynch-Stieglitz, J. (2003). Glacial-interglacial dynamics of the eastern equatorial Pacifc cold tongue-Intertropical convergence Zone system reconstructed from oxygen isotope records. Paleoceanography, 18(4).
Labeyrie, L., Labracherie, M., Gorfti, N., Pichon, J. J., Vautravers, M., Arnold, E., . . . Turon, J. L. (1996). Hydrographic changes of the southern ocean (southeast Indian sector) over the last 230 kyr (vol, 11, pg 57, 1996). Paleoceanography, 11(6), 813-814. doi:10.1029/96pa01490
Lamy, F., Gersonde, R., Winckler, G., Esper, O., Jaeschke, A., Kuhn, G., . . . Kilian, R. (2014). Increased Dust Deposition in the Pacific Southern Ocean During Glacial Periods. Science, 343(6169), 403-407. doi:10.1126/science.1245424
Lao, Y. (1991). Transport and burial rates of10Be and 231Pa in the Pacific Ocean. (PhD Thesis), Columbia University.
Lea, D. W., Pak, D. K., Belanger, C. L., Spero, H. J., Hall, M. A., & Shackleton, N. J. (2006). Paleoclimate history of Galapagos surface waters over the last 135,000 yr. Quaternary Science Reviews, 25, 1152-1167. doi:10.1016/jquascirev.2005.11.010
Lippold, J., Gherardi, J. M., & Luo, Y. M. (2011). Testing the Pa-231/Th-230 paleocirculation proxy: A data versus 2D model comparison. Geophysical Research Letters, 38, 7. doi:L20603 10.1029/2011gl049282
Lippold, J., Grutzner, J., Winter, D., Lahaye, Y., Mangini, A., & Christl, M. (2009). Does sedimentary Pa-231/Th-230 from the Bermuda Rise monitor past Atlantic Meridional Overturning Circulation? Geophysical Research Letters, 36, 6. doi:L12601 10.1029/2009gl038068
Lippold, J., Gutjahr, M., Blaser, P., Christner, E., M-L Carvalho Ferreira, Mulitza, S., . . . Jaccard, S. (2016). Deep water provenance and dynamics of the (de)glacial Atlantic meridional overturning circulation. Earth and Planetary Science Letters, submitted.
Lippold, J., Luo, Y., Francois, R., Allen, S. E., Gherardi, J., Pichat, S., . . . Schulz, H. (2012a). Strength and geometry of the glacial Atlantic Meridional Overturning Circulation. Nature Geoscience, 5(11), 813-816. doi:10.1038/ngeo1608
Lippold, J., Mulitza, S., Mollenhauer, G., Weyer, S., Heslop, D., & Christl, M. (2012b). Boundary scavenging at the East Atlantic margin does not negate use of Pa-231/Th-230 to trace Atlantic overturning. Earth and Planetary Science Letters, 333, 317-331. doi:10.1016/j.epsl.2012.04.005
Loubere, P., Mekik, F., Francois, R., & Pichat, S. (2004). Export fluxes of calcite in the eastern Equatorial Pacific from the last glacial maximum to the present. Paleoceanography, 19(PA2018).
Lyle, M. (1988). Climatically-forced organic carbon burial in the equatorial Atlantic and Pacific Oceans. Nature, 335, 529-532.
Marcantonio, F., Anderson, R. F., Higgins, S., Fleisher, M. Q., Stute, M., & Schlosser, P.

(2001). Abrupt intensification of the SW Indian Ocean monsoon during the last deglaciation: constraints from Th, Pa, and He isotopes. Earth and Planetary Science Letters, 184(2), 505-514. doi:10.1016/s0012-821x(00)00342-3

Marcantonio, F., Lyle, M., & Ibrahim, R. (2014). Particle sorting during sediment redistribution processes and the effect on 230Th-normalized mass accumulation rates. Geophysical Research Letters, - 41(- 15).

Martinez-Garcia, A., Rosell-Mele, A., Geibert, W., Gersonde, R., Masque, P., Gaspari, V., & Barbante, C. (2009). Links between iron supply, marine productivity, sea surface temperature, and CO2 over the last 1.1 Ma. Paleoceanography, 24. doi:Pa1207
10.1029/2008pa001657

McGee, D., deMenocal, P. B., Winckler, G., Stuut, J. B. W., & Bradtmiller, L. I. (2013). The magnitude, timing and abruptness of changes in North African dust deposition over the last 20,000 yr. Earth and Planetary Science Letters, 371, 163-176. doi:10.1016/j.epsl.2013.03.054

McGee, D., Marcantonio, F., & Lynch-Stieglitz, J. (2007). Deglacial changes in dust flux in the eastern equatorial Pacific. Earth and Planetary Science Letters, 257, 215-230.

Meckler, A. N., Sigman, D. M., Gibson, K. A., Francois, R., Martinez-Garcia, A., Jaccard, S. L., . . . Haug, G. H. (2013). Deglacial pulses of deep-ocean silicate into the subtropical North Atlantic Ocean. Nature, 495(7442), 495-+. doi:10.1038/nature12006

Mollenhauer, G., Schneider, R. R., Muller, P. J., Spiess, V., & Wefer, G. (2002). Glacial/interglacial variablity in the Benguela upwelling system: Spatial distribution and budgets of organic carbon accumulation. Global Biogeochemical Cycles, 16(4). doi:1134
10.1029/2001gb001488

Moore, T. C. B., L.H.; Geitzenauer,K.; luz,B.; Molina-Cruz,A.; Robertson,J.H.; Sachs,H.; Sanetta,C.; Thiede,J.; Wenkam,C. (1980). The reconstruction of sea surface temperatures in the Pacific Ocean of 18 000 B.P. Marine Micropaleontology, 5, 215-247.

Moran, S. B., & al, e. (2005). 231Pa and 230Th in surface sediments of the Arctic Ocean: Implications for 231Pa/230Th fractionation, boundary scavenging and advective transport. Earth and Planetary Science Letters, 234, 235-248.

Mulitza, S., Prange, M., Stuut, J.-B., Zabel, M., Dobeneck, T. v., Itambi, A. C., . . . Wefer, G. (2008). Sahel megadroughts triggered by glacial slowdowns of Atlantic meridional overturning. . Paleoceanography, 23. doi:10.1029/2008PA001637

Negre, C., Zahn, R., Thomas, A. L., Masque, P., Henderson, G. M., Martinez-Mendez, G., . . . Mas, J. L. (2010). Reversed flow of Atlantic deep water during the Last Glacial Maximum. Nature, 468(7320), 84-+. doi:10.1038/nature09508

Pisias, N. G., & Mix, A. C. (1997). Spatial and temporal oceanographic variability of the eastern equatorial Pacific during the late Pleistocence: Evidence from Radiolaria microfossils. Paleoceanography, 12(3), 381-393.

Pourmand, A., Marcantonio, F., Bianchi, T. S., Canuel, E. A., & Waterson, E. J. (2007). A 28-ka history of sea surface temperature, primary productivity and planktonic community variability in the western Arabian Sea. Paleoceanography, 22(4). doi:10.1029/2007pa001502

Pourmand, A., Marcantonio, F., & Schulz, H. (2004). Variations in productivity and eolian fluxes in the northeastern Arabian Sea during the past 110 ka. Earth and Planetary Science Letters, 221(1-4), 39-54. doi:10.1016/s0012-821x(04)00109-8

Rea, D. K., & Leinen, M. (1988). ASIAN ARIDITY AND THE ZONAL WESTERLIES - LATE PLEISTOCENE AND HOLOCENE RECORD OF EOLIAN DEPOSITION IN THE NORTHWEST PACIFIC-OCEAN. Palaeogeography Palaeoclimatology Palaeoecology, 66(1-2), 1-8. doi:10.1016/0031-0182(88)90076-4

Robinson, L. F., Noble, T. L., & McManus, J. F. (2008). Measurement of adsorbed and total Th-232/Th-230 ratios from marine sediments. Chemical Geology, 252(3-4), 169-179. doi:10.1016/j.chemgeo.2008.02.015

Rühlemann, C., Frank, M., Hale, W., Mangini, A., Mulitza, S., Muller, P. J., & Wefer, G. (1996). Late Quaternary productivity changes in the western equatorial Atlantic: Evidence from Th-230-normalized carbonate and organic carbon accumulation rates. Marine Geology, 135(1-4), 127-152. doi:10.1016/s0025-3227(96)00048-5

Schiebel, R. (2002). Planktic foraminiferal sedimentation and the marine calcite budget (DOI 10.1029/2001GB001459). Global Biogeochemical Cycles, 16(4), 13.

Scholten, J. C., Fietzke, J., Mangini, A., Garbe-Schönberg, C. D., Eisenhauer, A., Schneider, R., & Stoffers, P. (2008). Advection and scavenging: Effects on (230)Th and (231)Pa distribution off Southwest Africa. Earth and Planetary Science Letters, 271(1-4), 159-169. doi:10.1016/j.epsi.2008.03.060

Serno, S., Winckler, G., Anderson, R. F., Hayes, C. T., McGee, D., Machalett, B., . . . Haug, G. H. (2014). Eolian dust input to the Subarctic North Pacific. Earth and Planetary Science Letters, 387, 252-263. doi:10.1016/j.epsl.2013.11.008

Shemesh, A., & Peteet, D. (1998). Oxygen isotopes in fresh water biogenic opal - Northeastern US Alleröd-Younger Dryas temperature shift. Geophysical Research Letters, 25(11), 1935-1938.

Singh, A. K., Marcantonio, F., & Lyle, M. (2011). Sediment focusing in the Panama Basin, Eastern Equatorial Pacific. Earth and Planetary Science Letters, 309, 33-44.

Stoner, J. S., Channell, J. E. T., Hodell, D. A., & Charles, C. D. (2003). A similar to 580 kyr paleomagnetic record from the sub-Antarctic South Atlantic (Ocean Drilling Program Site 1089). Journal of Geophysical Research-Solid Earth, 108(B5). doi:10.1029/2001jb001390

Thomas, A. L., Henderson, G. M., & McCave, I. N. (2007). Constant bottom water flow into the Indian Ocean for the past 140 ka indicated by sediment (231)Pa/(230)Th ratios. Paleoceanography, 22(4). doi:10.1029/2007pa001415

Thompson, P. (1981). Planktonic Foraminifera in the western North Pacific druring the past 150 000 years: comparison of modern and fossil assembledges. Palaeogeography, Palaeoclimatology, Palaeoecology, 35, 241-279.

Vidal, L., Schneider, R. R., Marchal, O., Bickert, T., Stocker, T. F., & Wefer, G. (1999). Link between the North and South Atlantic during the Heinrich events of the last glacial period. Climate Dynamics, 15(12), 909-919. doi:10.1007/s003820050321

Walter, H. J., Rutgers van der Loeff, M. M., & Hoeltzen, H. (1997). Enhanced scavenging of 231Pa relative to 230Th in the South Atlantic south of the Polar Front: Implications for the use of the 231Pa/230Th ratio as a paleoproductivity proxy. Earth and Planetary Science Letters, 149(1,Äì4), 85-100. doi:http://dx.doi.org/10.1016/S0012-821X(97)00068-X

Winckler, G., Anderson, R. F., Fleischer, M. Q., McGee, D., & Mahowald, N. (2008). Covariant Glacial-Interglacial dust fluxes in the Equatorial Pacific and Antarctica. Science, 320, 93-96.

Yang, Y.-L., Elderfield, H., Pedersen, T., & Ivanovich, M. (1995). Geochemical record of the Panama basin during the last glacial maximum carbon event shows that the glacial ocean was not suboxic. Geology, 23(12), 1115-1118.

Table 1: Model runs and statistical correlations (spearman's rho) to ThoroMap in the 0-4 ka and 19-23 ka time slice. Sites included in the model-data correlation do not include any sites that have previously been used to tune the models. The numbers of all screened sites in ThoroMap is given in brackets.

model	scenario	time	model reference	sites	rho
CCSM4	Cf4n_2k	2 ka	Albani et al. 2015	135 (157)	0.59
CCSM3	SMOB	current	Mahowald et al. 2006	148 (157)	0.63
CCSM4	Cf4n_lgm	19-23 ka	Albani et al. 2014	54 (76)	0.83
CCSM3	SMOB_lgm	19-23 ka	Mahowald et al. 2006	67 (76)	0.82

Figure Captions

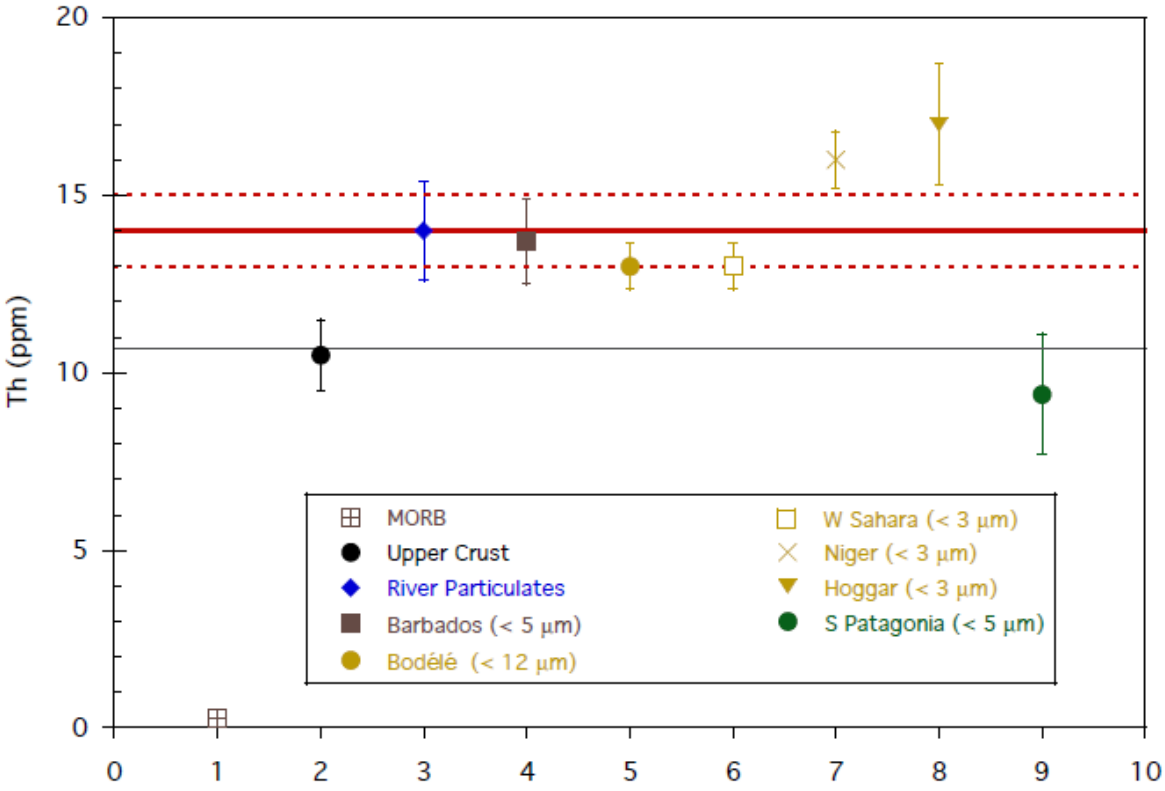

Figure 1: Th concentration in fresh Mid-Ocean Ridge Basalt (MORB, n=34, Kelemen 2004) compared to the composite value for upper crust based on extensive analysis of sediments and loess deposits (Gao and Rudnick, 2004). Black line indicates an earlier estimate of the average Th concentration in upper crust (10.7 ppm; Talor and McLennan, 1985), which has previously been used for dust reconstructions using ^{232}Th. Red line shows the recently recommended value (14 ± 1 ppm), which is the error weighted mean Th concentration in fine (<5 µm) samples from all global dust source areas except Patagonia (McGee et al. 2016). Th data from suspended particulates collected in the world's largest rivers systems (n=10) are from Martin and Meybeck (1979). Remaining points show Th concentrations in the fine fraction of African dust from Barbados (<5 µm, n=8, Muhs et al. 2007), sediment and eolian deposits from the Bodélé Depression in Chad (< 12 µm, n=1), the western Sahara coastal region (< 3 µm, n=1), southwest Niger (< 3 µm, n=1), the Hoggar Massif in Algeria (< 3 µm, n=1; *all African data from* Castillo et al., 2008) and from Patagonia (< 5 µm, n=7, McGee et al., 2016). See SPM dataset 1 for details**.**

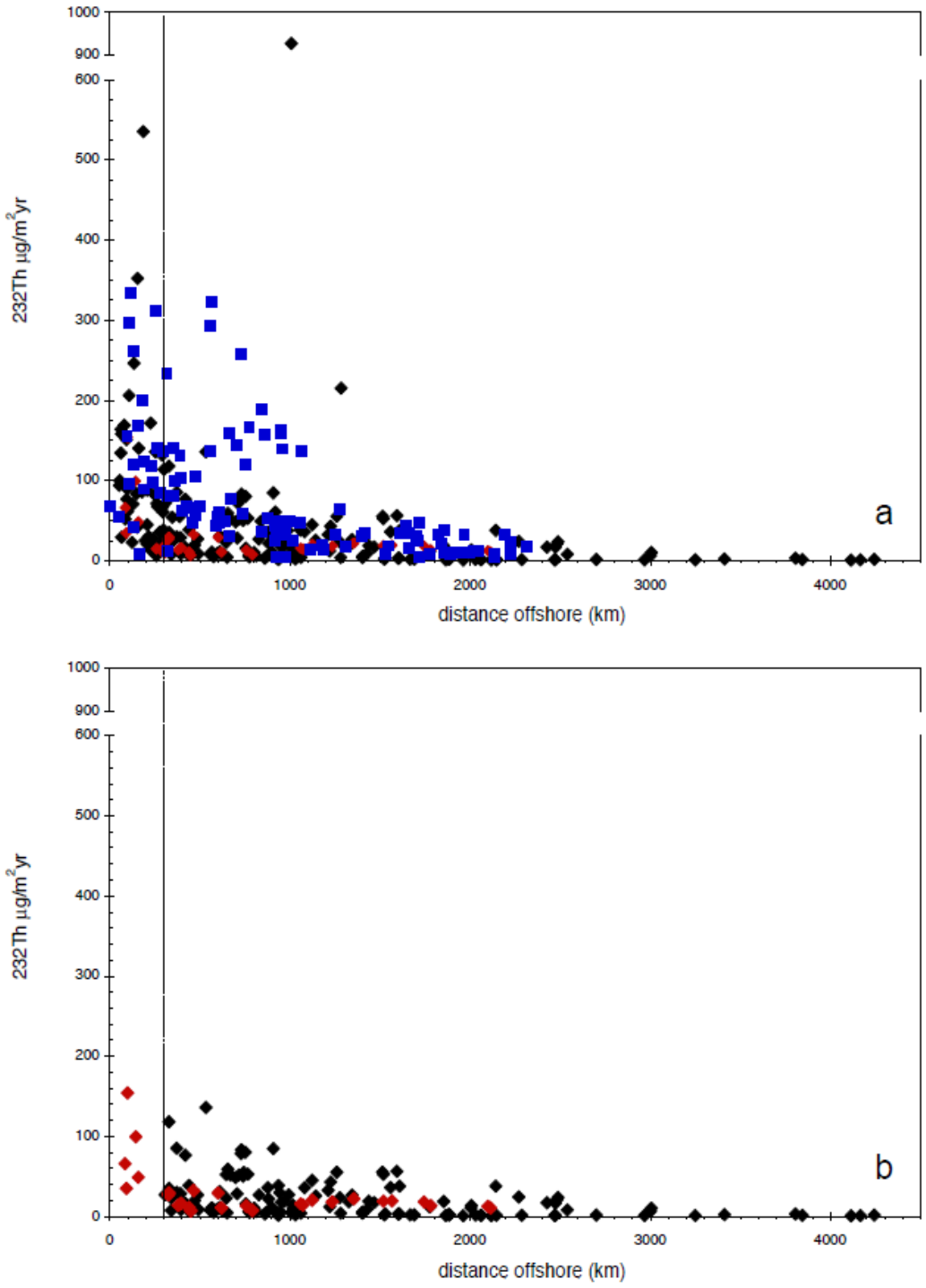

Figure 2: Thorium-232 fluxes (0-4 ka) plotted against distance offshore for the a) full and b) screened database in units of µg/m^{2}yr. Sites from latitudes more polar than 50° (Southern Ocean, North Atlantic) and 55° (North Pacific) are in shown in blue squares; sites for which corrections have been applied to isolate the eolian signal from other continental inputs in the original references are in red. Note gap in y-axis. See SPM for data sources.

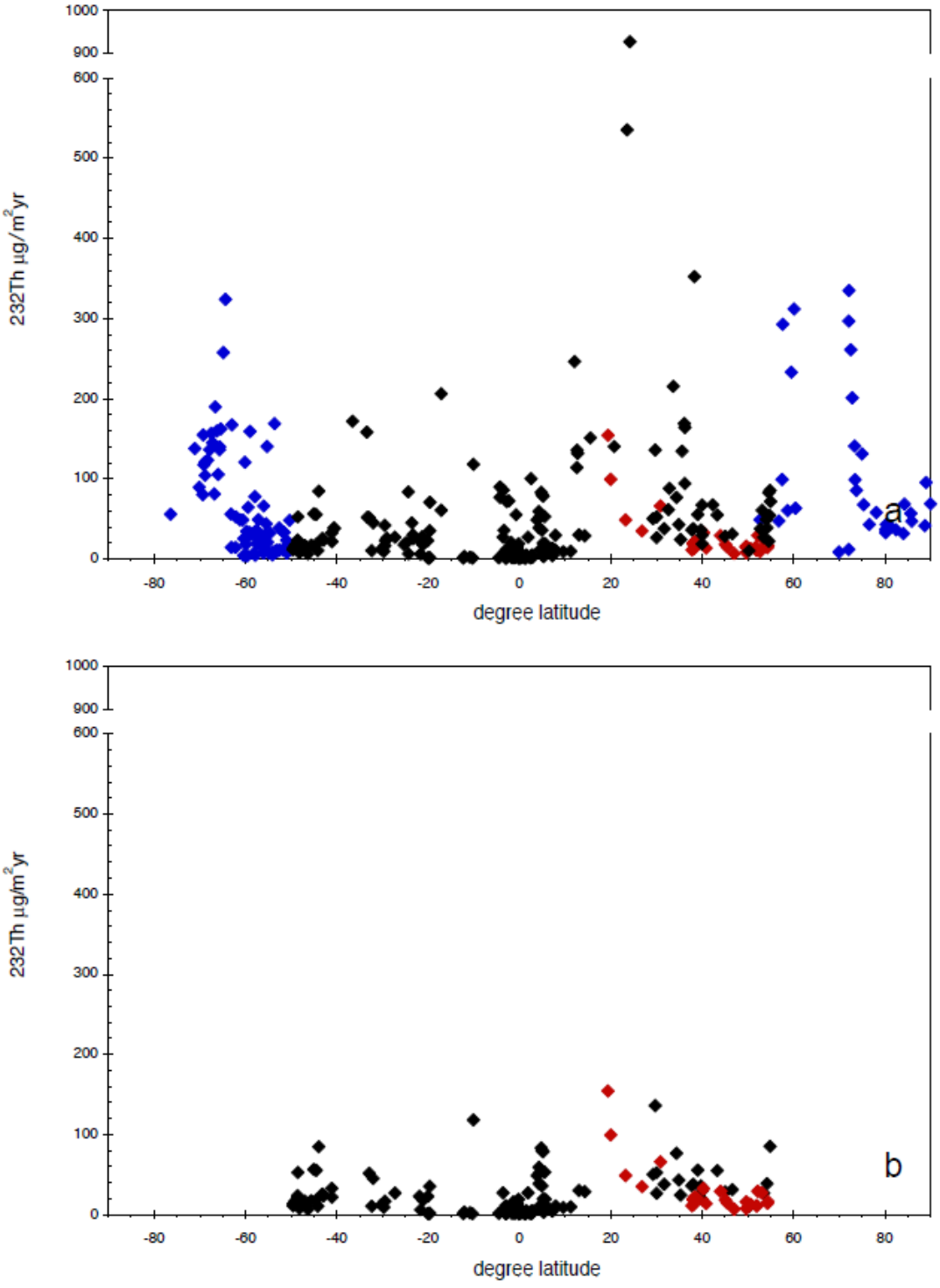

Figure 3: Thorium-232 fluxes (0-4 ka) plotted against latitude for the a) full and b) screened database in units of µg/m^{2}yr. See Figure 2 for symbol colors.

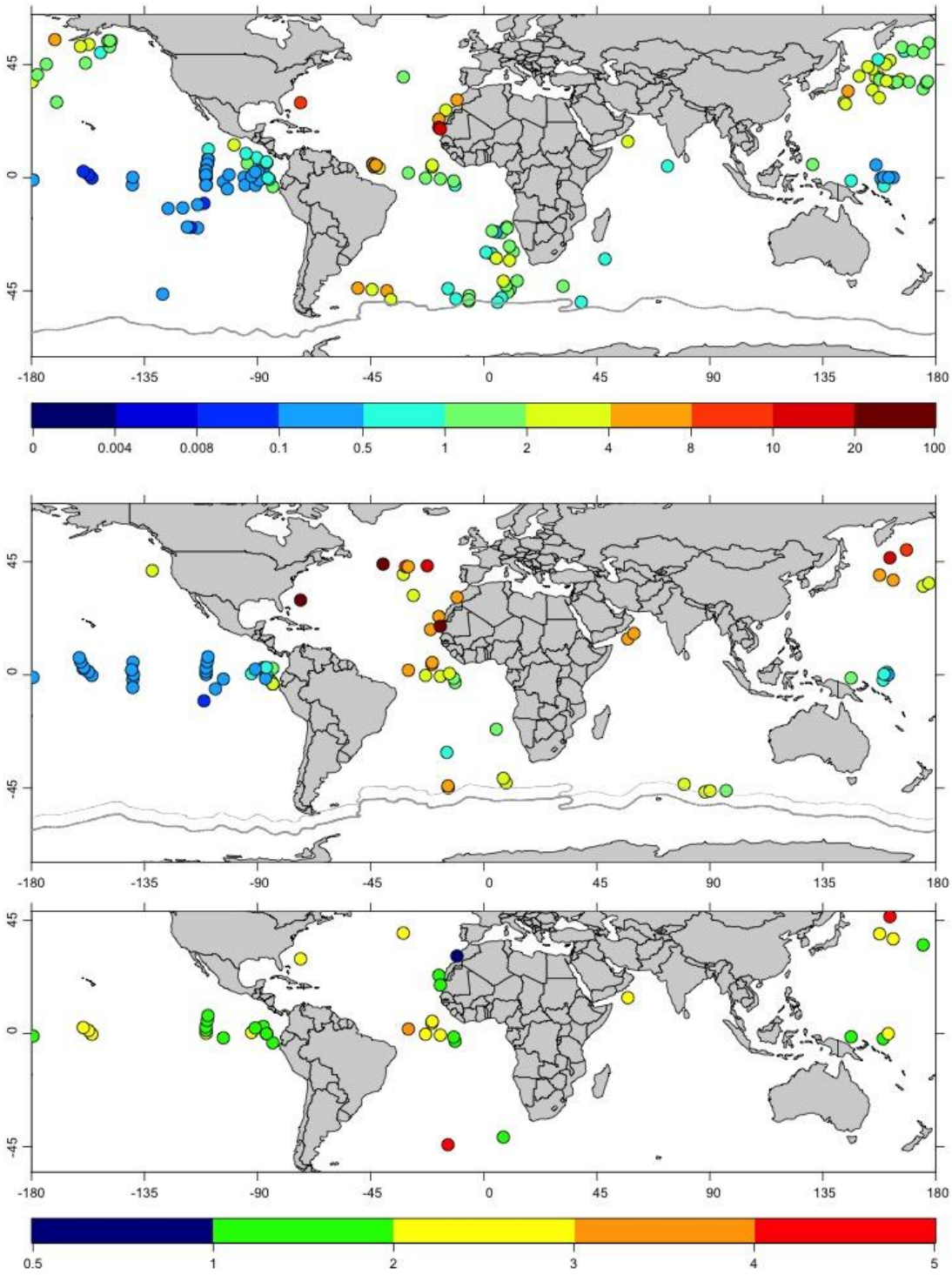

Figure 4: ThoroMap dust deposition (g/m^{2}yr) in the late Holocene (0-4 ka, top) and the LGM (19-23 ka, middle). Note non-linear color bar. The position of the modern Polar Front (Orsi et al., 1995) is indicated in grey (*top*, *middle*) and has been shifted north by 5°(*middle*). LGM/late Holocene ratios are shown in the bottom panel.

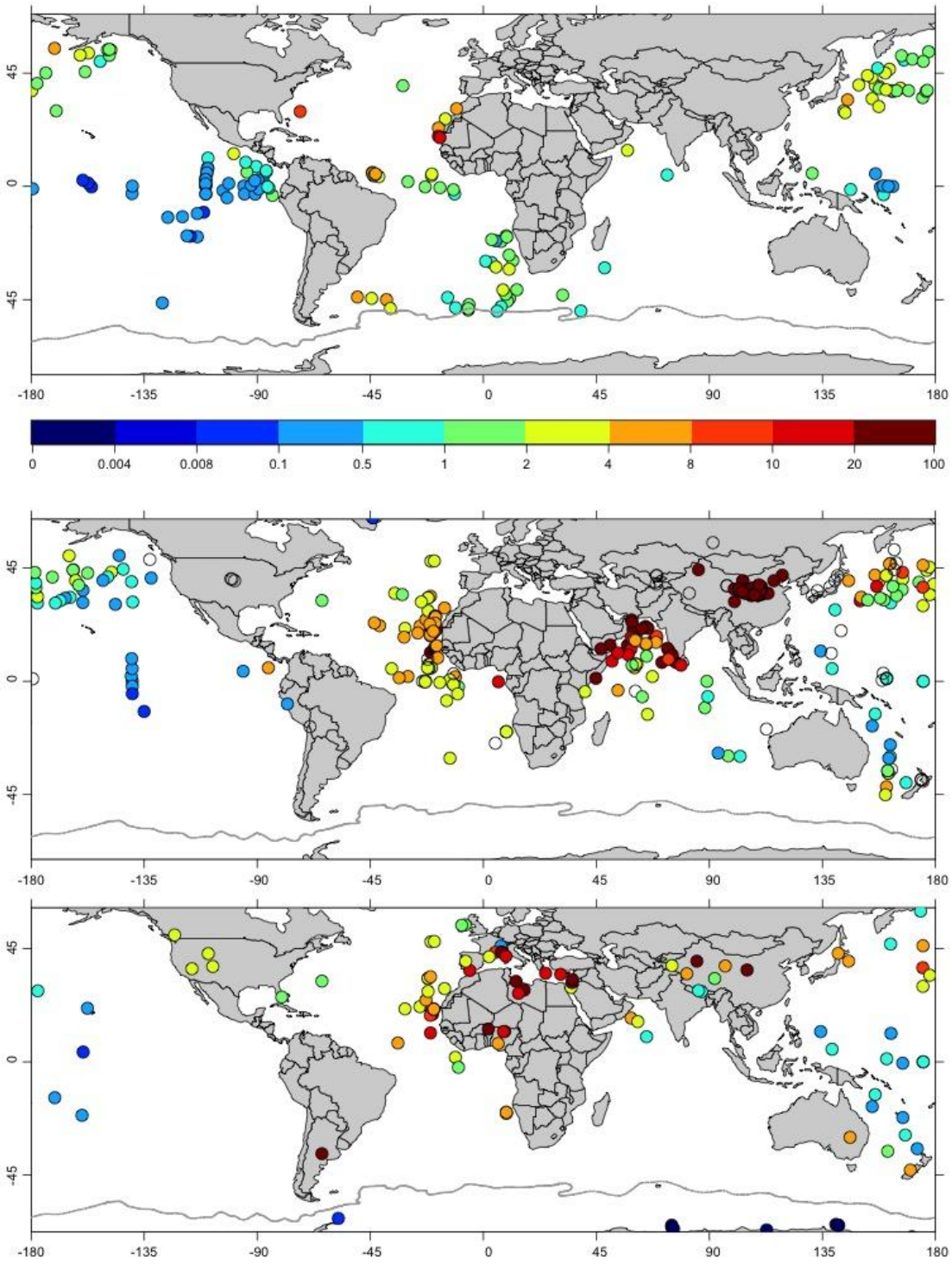

Figure 5: ThoroMap dust deposition (g/m^2yr) for the late Holocene (0-4 ka, *top*) compared to DIRTMAP-2 (0-10 ka, Kohfeld, 2002) and the observational database of modern dust deposition (≤ 10 μm) by Albani et al. 2014. The position of the modern Polar Front (Orsi et al., 1995) is indicated in grey.

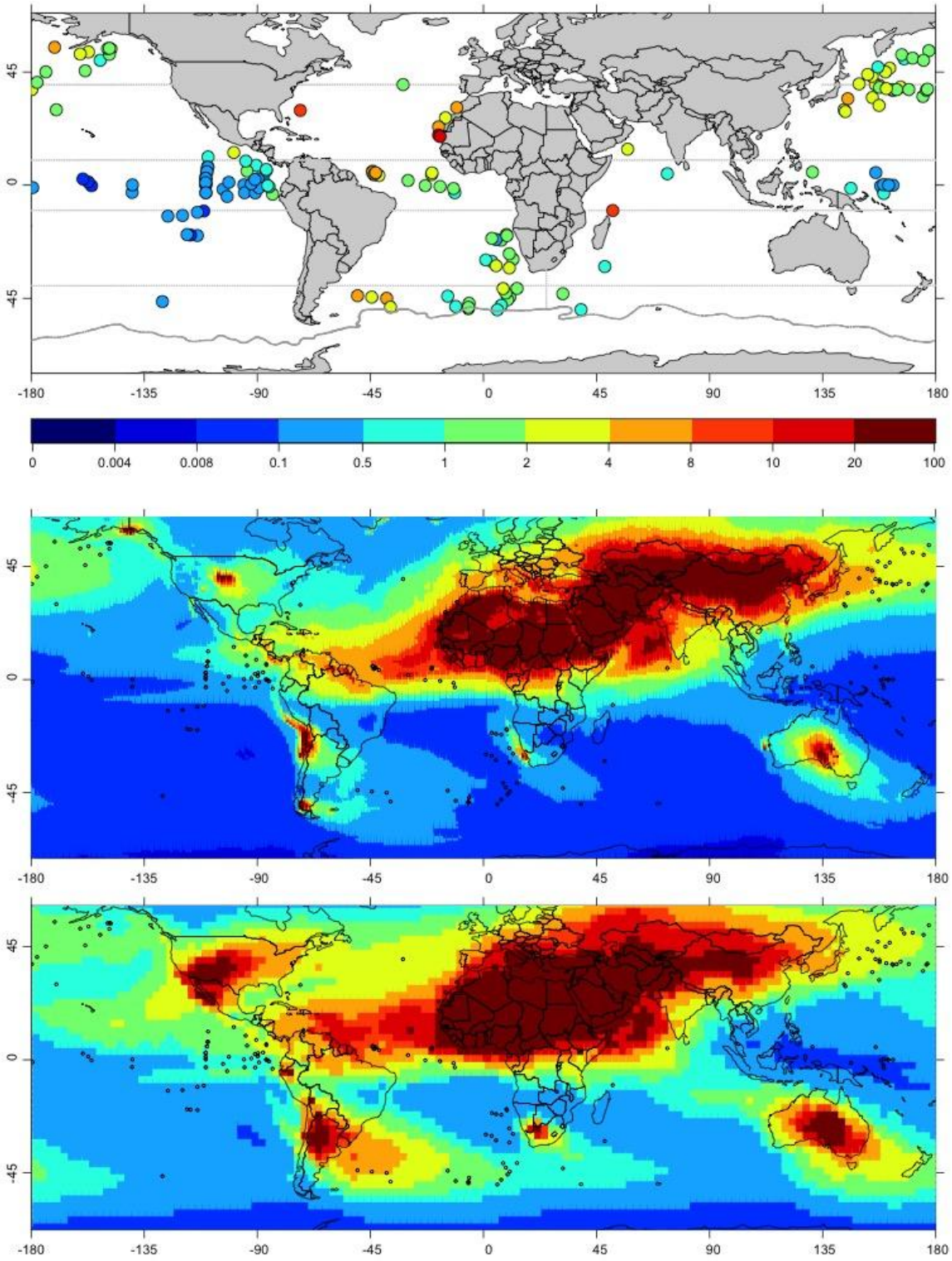

Figure 6: ThoroMap dust deposition (g/m^2yr) for the late Holocene (0-4 ka, *top*) compared to CCSM4 (case C4fn_2k; *middle*) and CCSM3 (case SMOB, *bottom*). Note non-linear color bar. The position of the modern Polar Front (Orsi et al., 1995) is indicated in grey (*top*). Zonal grey lines (*top*) delineate the regions discussed in text and Fig. 7.

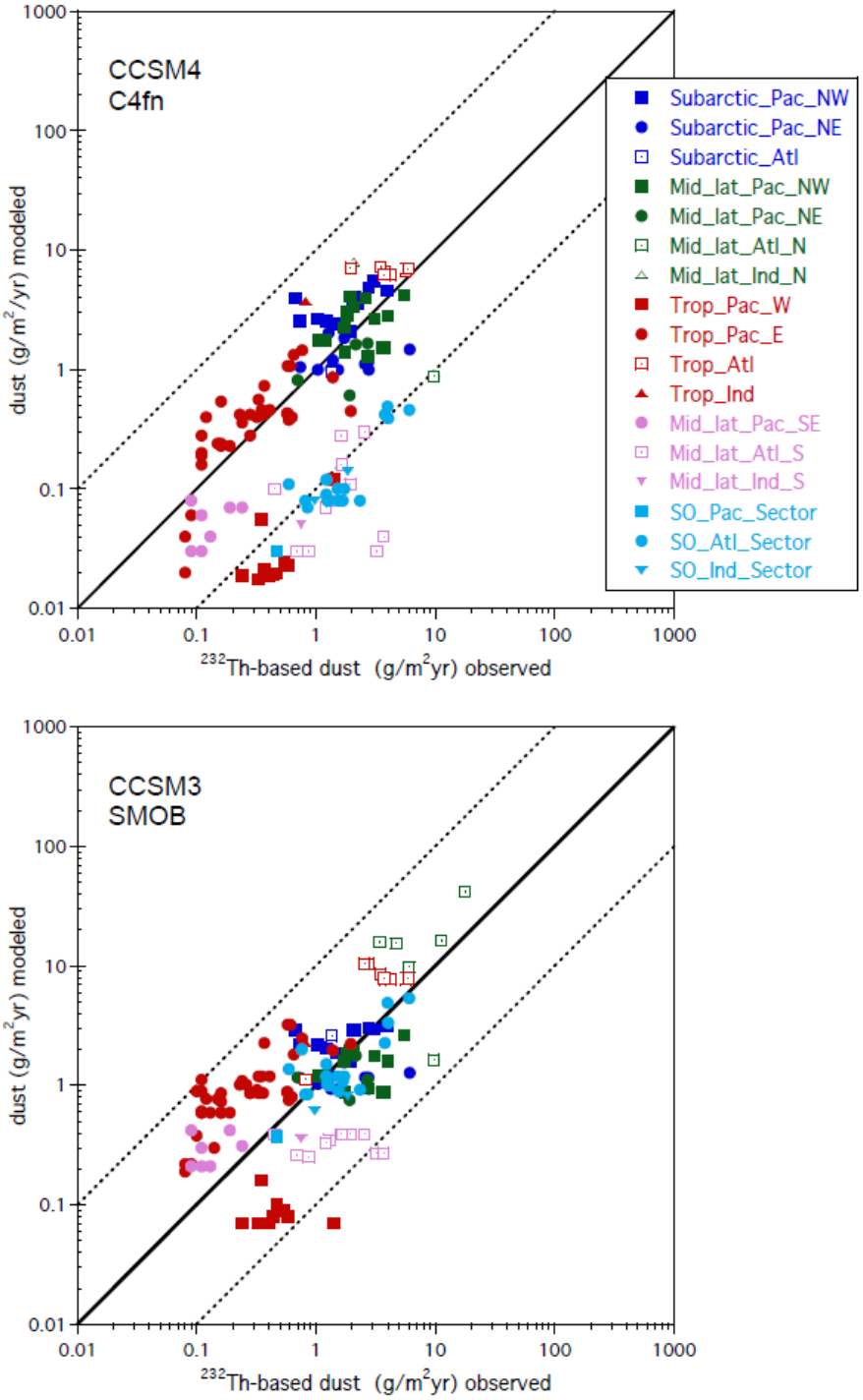

Figure 7: ThoroMap (0-4 ka) plotted against CCSM4 (*top*) and CCSM3 (*bottom*). Symbols are color-coded according to latitude and ocean basin (see lines in Fig. 6 *top*). Subarctic sites originate from 40-50°N in the Atlantic and 40-55°N in the Pacific. Mid-latitude sites originate from 40-10°N and 40-10°S, tropical sites are from 10°S-10°N, Southern Ocean sites originate from 40-50°S. Sites that have used previously to tune the models are excluded.

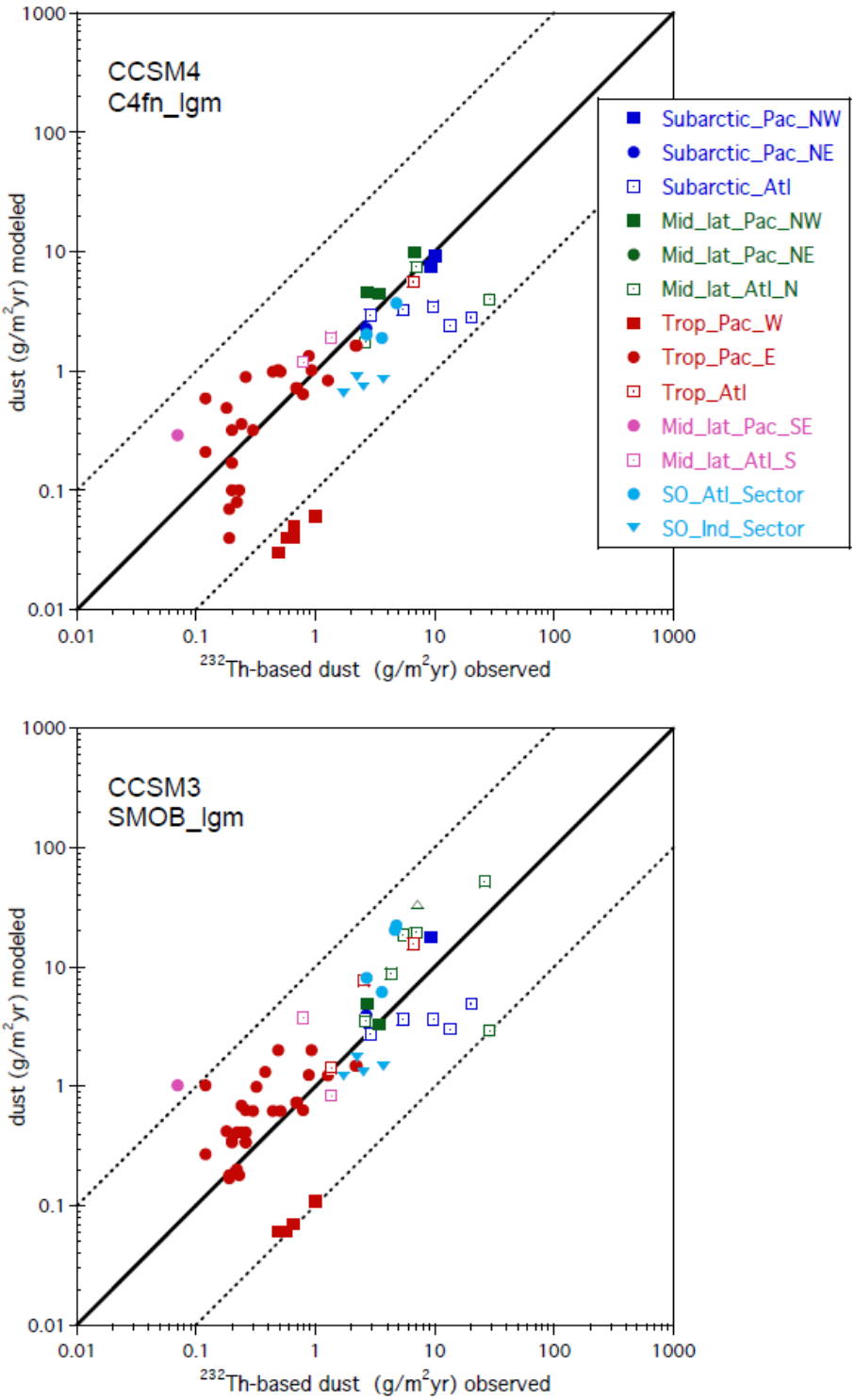

Figure 8: ThoroMap (19-23 ka) plotted against CCSM4 (top) and CCSM3 (bottom). Symbols are color-coded according to latitude and ocean basin (see lines in Fig. 6 top, and Fig.7 caption). Sites that have been used previously to tune the models are excluded.